BM@N Run6 Analysis Note v.3
Production of Λ hyperons in 4.0 and 4.5 AGeV carbon-nucleus interactions at the Nuclotron

Analysis team: M. Kapishin[1], A. Zinchenko[1], I. Rufanov[1], M. Zavertyaev[2], V. Vasendina[1], G. Pokatashkin, Yu. Stepanenko[1,3,*], K. Alishina[1]

[1] Joint Institute for Nuclear Research, Dubna, Moscow region, 141980, Russia
[2] Lebedev Physical Institute of the Russian Academy of Sciences, Moscow, 119991, Russia
[3] Gomel State University, Gomel, 246019, Belarus
*e - mail: yystepanenko@gmail.com

for BM@N Collaboration
June 2024

Abstract

Production of Λ hyperons in interactions of the carbon beam with the kinetic energy 4.0 and 4.5 AGeV with the C, Al, Cu, Pb targets was studied with the BM@M detector at the Nuclotron. The analysis procedure is described in details. Results on Λ hyperons yields have been obtained and compared with the model predictions and another experiments.

BM@N configuration in the carbon beam run

The technical run of the BM@N detector was performed with the carbon beam in March 2017. The view of the BM@N setup used in the run is presented in Fig. 1 (left). The configuration of the central tracker was based on one plane of a forward silicon detector and six GEM stations combined from 5 GEM detectors with the size of 66x41 cm^2 and 2 GEM detectors with the size of 163x45 cm^2 [2]. More detailed configuration of the GEM detectors described in [1]. The tracking stations were arranged to have the beam passing through their centers (Fig. 1 (right)). Each successive GEM station was rotated by 180^o around the vertical axis. It was done to have the opposite electron drift direction in the successive stations in order to avoid a systematic shift of reconstructed tracks due to the Lorentz angle in the magnetic field. The research program was devoted to measurements of inelastic reactions $C+A\rightarrow X$ with the beam kinetic energy of 4.0 and 4.5A GeV and different targets: *C, Al, Cu, Pb*. The technical program of the run included the measurement of the carbon beam momentum in the central and outer tracker at different values of the magnetic field. Since the GEM tracker configuration was tuned to measure relatively high-momentum beam particles, the geometric acceptance for relatively soft decay products of strange *V0* particles was rather low.

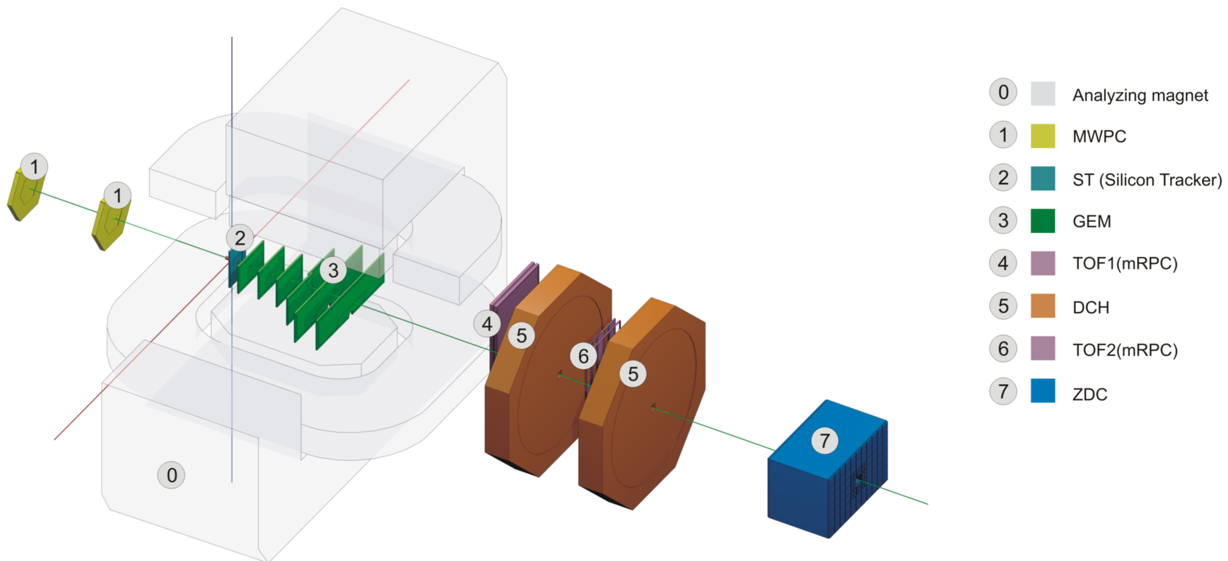

Figure 1. BM@N set-up in the carbon beam run (Run6)

In the present analysis the experimental data from the forward silicon detector, GEM detectors, trigger barrel multiplicity detector, beam, veto and T0 counters were used. The positions of the beam counters and trigger barrel detector and the target are given in Fig.2. The carbon beam intensity was few 10^5 per the spill, the spill duration was 2-2.5 sec. The magnetic field in the center of the analyzing magnet was 0.61 T.

Monte-Carlo simulation and event reconstruction

The Monte-Carlo (MC) event samples of *C+A* collisions were produced with the DCM-QGSM event generator. The passage of particles through the setup volume was simulated with the GEANT4 program integrated into the BmnRoot software framework. To properly describe the GEM detector response in the magnetic field the microsimulation package Garfield++ was used.

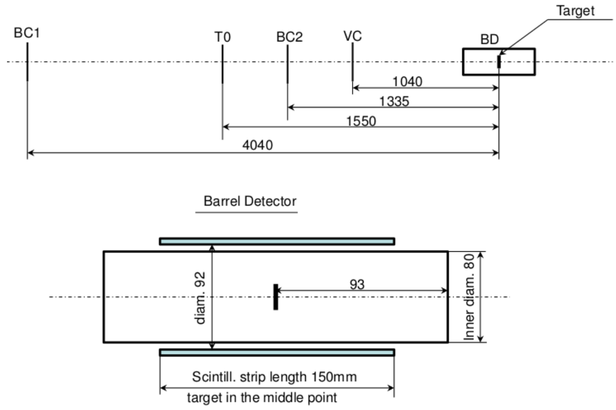

Figure 2. Schematic view and positions of the beam counters, barrel detector and target.

The package gives detailed description of the processes inside the GEM detector, including the drift and diffusion of released electrons in electric and magnetic fields and the electron multiplication in GEM foils, so that the output signal from the readout plane can be reproduced. To speed up the simulation, dependencies of the Lorentz shifts and the charge distributions on the readout planes on the drift distance were parameterized and used in the GEM digitization part of the BmnRoot package. The details of the detector alignment, Lorenz shift corrections are described in the paper [3]. The track reconstruction method was based on the so-called “cellular automaton" approach [4]. The tracks found were used to reconstruct primary and secondary vertices using the “KF-particle" formalism [5].

Track selection criteria

The total number of the statistics involved to the analysis was ~2.9×10^7 for the physical data and ~3.8×10^7 for Monte-Carlo simulation (for each target and energy). The Λ hyperons events candidates were reconstructed using their decay mode into two oppositely-charged tracks. Since particle identification was not used in the analysis, all positive tracks were considered as protons and all negative as π^-.

The tracks selection criteria were:

1. Number of tracks in selected events: positive>=1, negative>=1;
2. Beam halo, pile-up suppression within the readout time window: number of signals in the start detector: T0=1, number of signals in the beam counter: BC2=1, number of signals in the veto counter around the beam: Veto=0;
3. Trigger condition in the barrel detector: number of signals BD>=2 or BD>=3 (energy and target dependent);

Table 1. ε_{pileup} suppression factors.

Selection	4 AGeV	4.5 AGeV
T0==1	+	+
BC2==1	+	+
Veto==0	+	+
C	0.674±0.034	0.529±0.026
Al	0.740±0.037	0.618±0.031

Cu	0.779±0.039	0.621±0.031
Pb	0.784±0.039	0.686±0.034

The suppression factors of reconstructed events ε_{pileup} due to selection criteria 2 applied to suppress beam halo and pile-up events in interactions of the 4.0 and 4.5 AGeV carbon beam with the *C, Al, Cu, Pb* targets are given in Table 1. The total number of triggered events, the beam fluxes and luminosities are summarized in Table 2.

Table 2. Number of triggered events, beam fluxes and integrated luminosities collected in interactions of the carbon beam of 4.0 and 4.5AGeV with different targets.

Interactions, target thickness	Number of triggers / 10^6	Integrated beam flux / 10^7	Integrated luminosity / 10^{30} cm^{-2}
4 AGeV, *C+C* (9 mm)	4.04	6.07	6.06
4 AGeV, *C+Al* (12 mm)	4.61	3.31	2.39
4 AGeV, *C+Cu* (5 mm)	4.87	4.71	2.00
4 AGeV, *C+Pb* (10 mm)	0.81	0.67	0.22

Interactions, target thickness	Number of triggers / 10^6	Integrated beam flux / 10^7	Integrated luminosity / 10^{30} cm^{-2}
4.5 AGeV, *C+C* (9 mm)	3.01	4.70	4.69
4,5 AGeV, *C+Al* (12 mm)	3.69	4.98	3.60
4.5 AGeV, *C+Cu* (5 mm)	5.44	7.21	3.06
4.5 AGeV, *C+Pb* (10 mm)	2.40	2.58	0.84

Monte-Carlo tuning

1. Gem's Efficiency

The two-dimensional (X, Y) efficiency distributions for six GEM station were calculated for the experimental data to reproduce the detector effects in the MC track reconstruction.

For each station they were estimated using the following approach:

1. Divide detectors area into 180x45 cells (along X and Y coordinates correspondently);
2. Select good quality tracks with the number of hits per track (excluding the station under study) not less than *N*;
3. Check that track crosses the detector area, if yes, add one track to the denominator;
4. If there is a hit in the detector, which belongs to the track, add one track to the numerator;
5. Detector efficiency = sum of tracks in numerator / sum of tracks in denominator.

Simulated amplitude signals in the GEM detectors were modified according to amplitudes of the experimental signals in these detectors. GEM (*X, Y)* efficiencies for data and mc are presented in Fig. 3 and Fig. 4. One-dimensional comparison GEM efficiencies between the experimental data and MC shown in Fig. 5. Discrepancies between data and MC do not exceed 10% range.

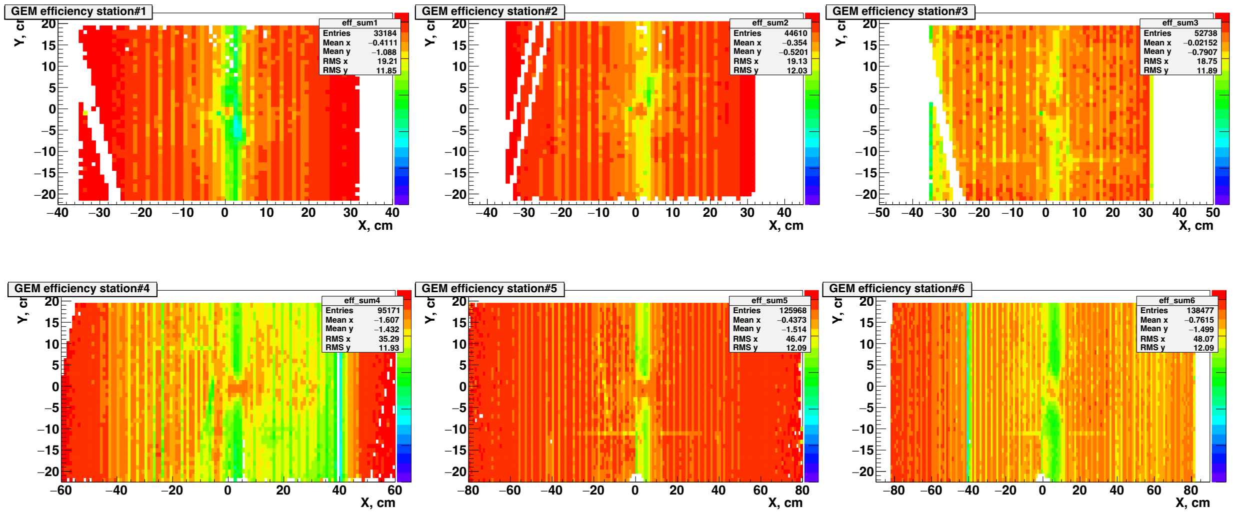

Figure 3. Two-dimensional *(X, Y)* efficiency distributions in six GEM stations measured with experimental tracks (C+C 4.0GeV process).

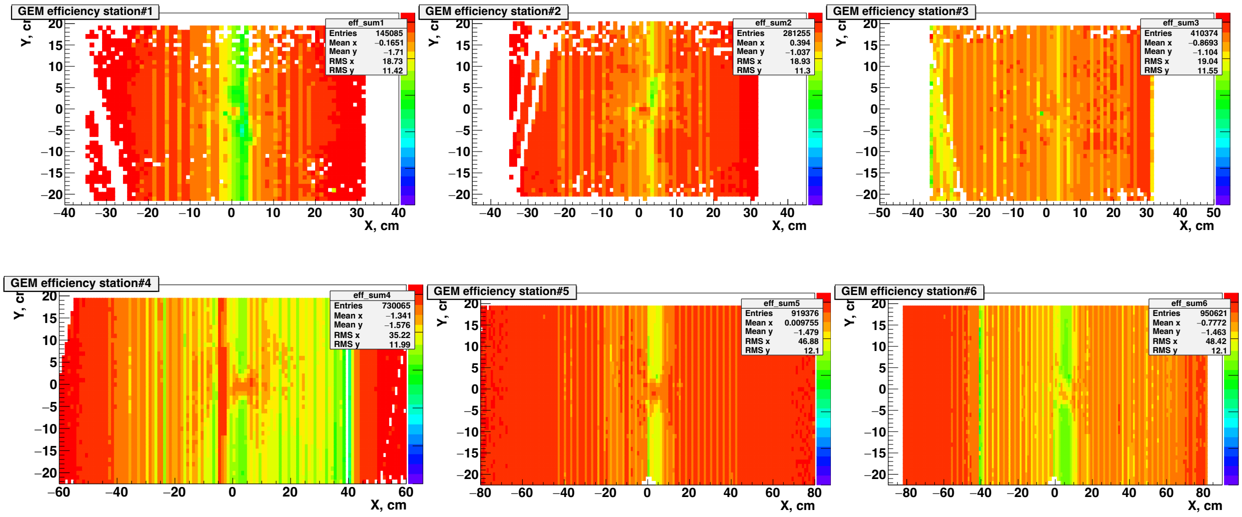

Figure 4. Two-dimensional *(X, Y)* efficiency distributions in six GEM stations implemented into Monte-Carlo simulation according to experimental data (C+C 4.0GeV process).

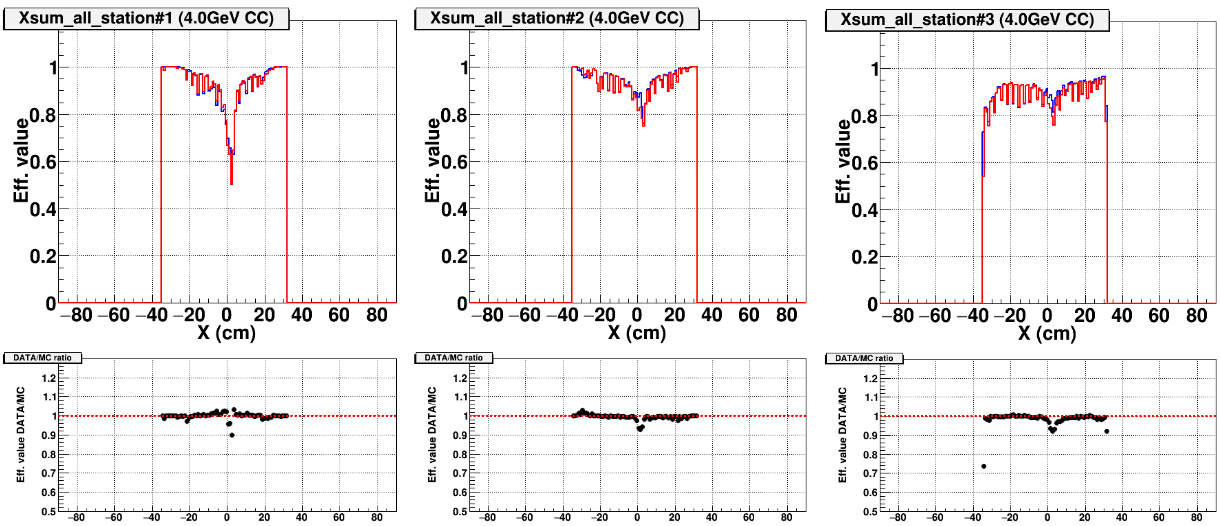

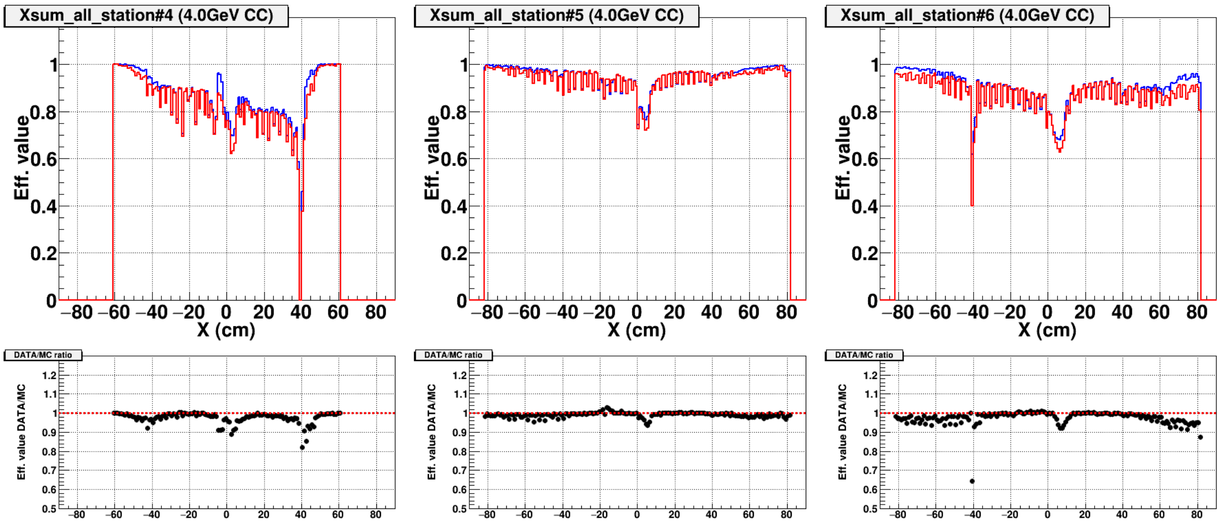

Figure 5. One-dimensional GEM efficiency comparison between the experimental data (red line) and MC (blue line). Pictures was obtained by integration along Y-axis. Black distributions correspond to the ratio of the data to MC distributions (C+C 4.0GeV process).

1. Track hits residual corrections

The dx -residual values and their corresponding errors were analyzed for each GEM station [6] for the MC samples and the physical data

The dx-residual value (and the same for dy-residual) corresponds to the difference between the x_{rec} hit coordinate of the reconstructed track and the x_{ext} hit coordinate of the extrapolated track in GEM station *z*-position. The x_{ext} value was calculated by excluding the reconstructed track hit from the considered GEM station and further extrapolation of this track to this GEM plane. The geometrical interpretation of the dx-residual is presented in Fig. 6, where $dx = (x_{rec} - x_{ext})$ is the value of dx-residual in considered GEM detector station.

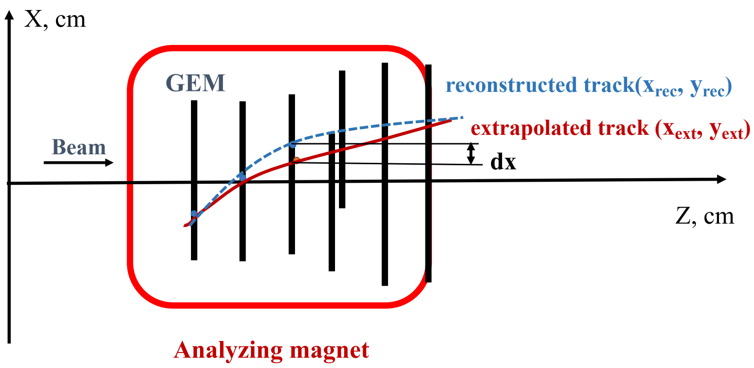

Figure 6. Geometrical definition of dx-residual value, where x_{rec} is reconstructed track x hit position and x_{ext} is extrapolated track x hit position in GEM station.

Tracks with at least four hits out of seven in the central tracker (GEM+Si detectors) were selected for the dx-residual analysis. The two-dimensional dependencies of the dx value versus x were calculated for each GEM station, where x corresponds to the extrapolated track hit coordinate (x_{ext}) in the detector plane Fig. 7. After that $dx(x)$ distributions were sliced along the x-axis for each GEM detector and one-dimensional dx-distributions were fitted using the sum of the second-order polynomial function and the Gaussian function (1.1) (Fig. 8):

$$F(dx)_{fit} = p_0 + p_1 dx + p_2 dx^2 + p_3 \exp\left(-\frac{1}{2}\left(\frac{dx - p_4}{p_5}\right)^2\right), \tag{1.1}$$

where: $p_0, \dots p_5$ are free parameters of the fit function;
dx - is the value of the residual.

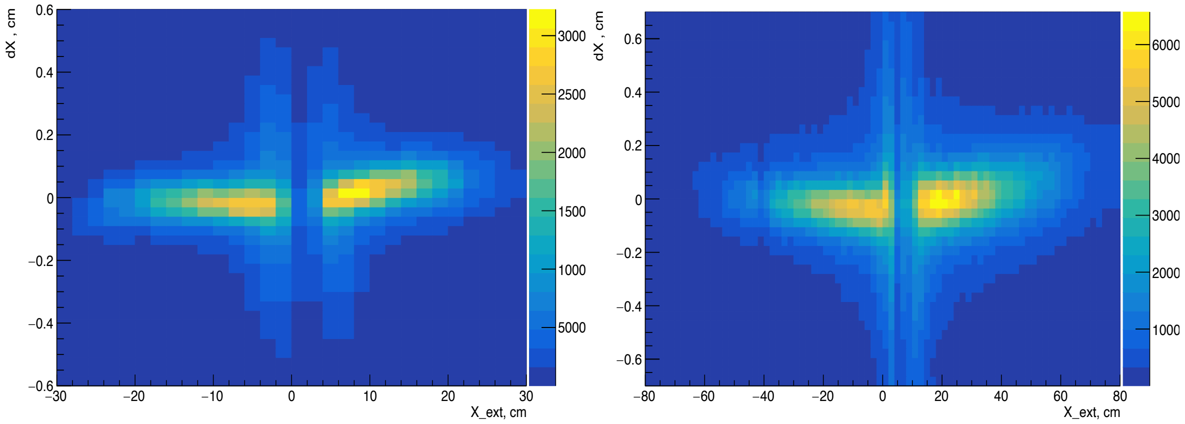

Figure 7. The two-dimensional $dx(x)$ distributions. C+Cu 4.0 AGeV data for 2nd (left) and 6th (right) stations.

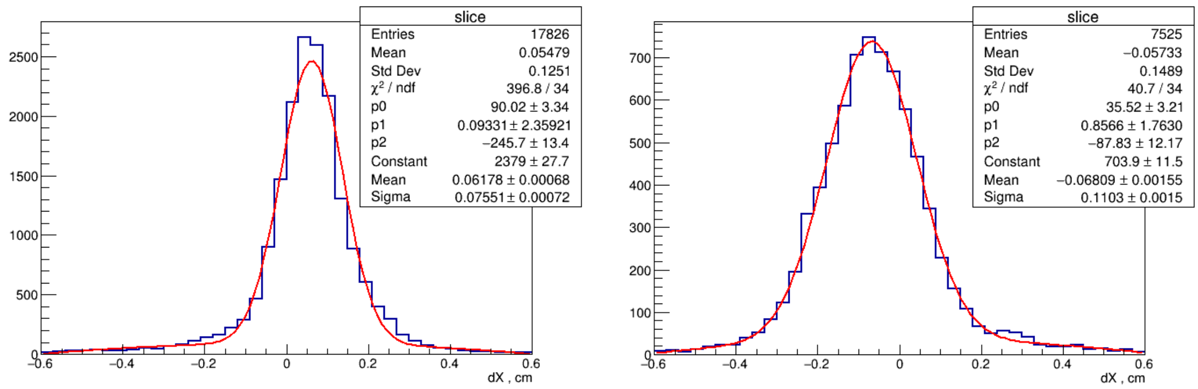

Figure 8. The one-dimensional sliced $dx(x)$ distributions with fit function (1.1). C+Cu 4.0 AGeV data, 2nd GEM station.

The values of the parameters p_4 (peak position of the Gaussian function) and p_5(width of the Gaussian function) which are correspond to the mean value position of the dx-residual and its determination error respectively were extracted from the fit. The distributions of the dx-residual mean position depending on the x coordinate for each GEM detector station are presented in blue square points in Fig. 9 and Fig. 10 for MC and data respectively.

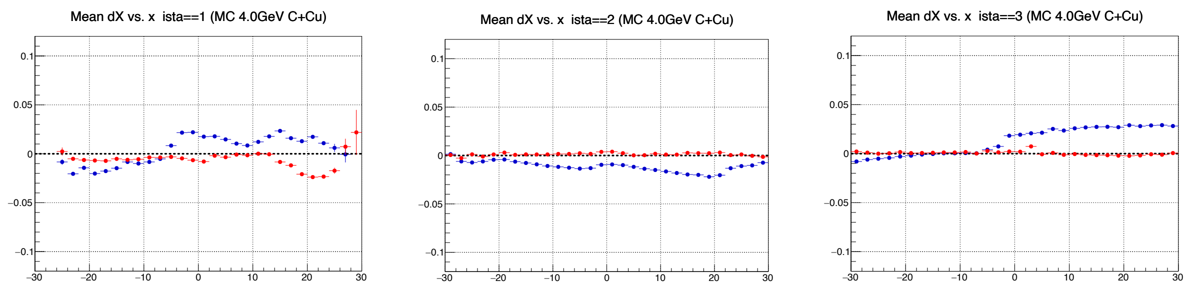

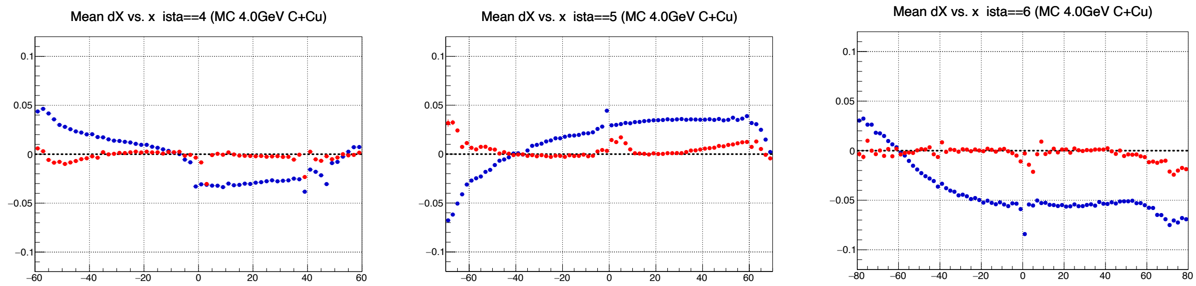

Figure 9. Mean dx-residuals vs. x for all GEM stations for MC. Blue square point to the mean dx-residuals before correction. Red triangle points to the mean dx-residuals after corrections. Reaction C + Cu, energy 4.0 GeV.

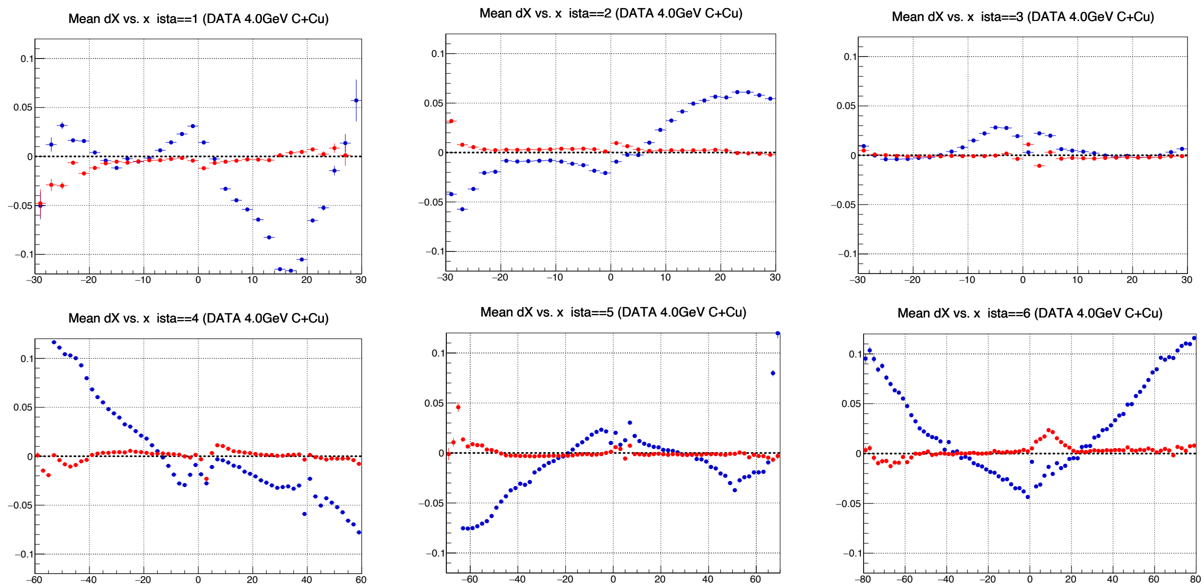

Figure 10. Mean dx-residuals vs. x for all GEM stations for experimental data. Blue square point to the mean dx-residuals before correction. Red triangle points to the mean dx-residuals after corrections. Reaction *C+Cu*, energy 4.0 GeV.

These distributions show that the position of the dx-residual mean values along the x-axis is not at zero positions; this suggest that the procedure of the track hits reconstruction in GEM detectors have discrepancies.

To improve the track hits reconstruction algorithm the iterative procedure of the dx-residual corrections was proposed and implemented. It consists of the following steps:

1. Calculate the dx-residual mean values depending on the x coordinate from the one-dimensional dx-distributions fits using (1.1) as described above;
2. Fit the $dx(x)$ distributions using two functions as (1.2) for positive and negative side of the detector along x coordinate;

$$F(x)_{fit} = p_0 + p_1 x + p_2 x^2 + p_3 x^3 + p_4 x^4 + p_5 x^5, \quad (1.2)$$

where: $p_0, \dots p_5$ are free parameters of the fit function;
x is coordinate of the track hit along the x-axis of the GEM station.

3. Make corrections of reconstructed x_{rec} values using functions (1.2) with extracted parameters from the fits (step 2) for positive and negative side of the detector along x coordinate: $x_{rec} = x_{rec} - 0.5 \cdot F(x)_{fit}$
4. Calculate new $dx(x)$ distributions (as in step 1);

5. Compare distributions before and after corrections;
6. Repeat dx-residual corrections procedure if necessary (steps 1-5).

The result of dx-residual corrections is presented in Figs. 9 and Fig. 10 in red points. It was obtained after applying dx-residual corrections algorithm two times. Distributions after corrections show that the accuracy of the reconstructed track hits coordinates (x_{rec}) in the GEM stations was improved as for data as for MC simulation.

The procedure of the track hit residual corrections was applied for all energies and targets in Run6 analysis.

2. Track hit position error corrections

After applying the track hits position correction procedure, the hit deviations from the reconstructed track was evaluated using physical data and corresponding corrections were applied in MC (parameter p_5 from 1.1) The result of the corrections is shown in Fig. 11 for dx-residuals and in Fig.12 for dy-residuals.

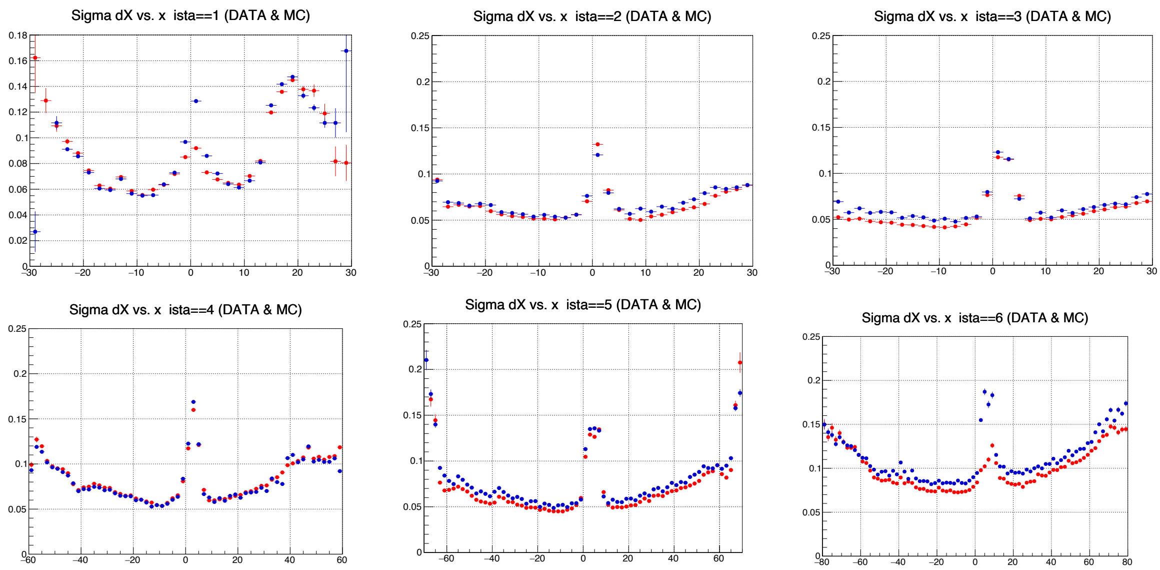

Figure 11. The error width of the dx-residuals determination vs. x for all GEM station after corrections. Blue points - MC, red points - data. Reaction C+Cu, energy 4.0 GeV.

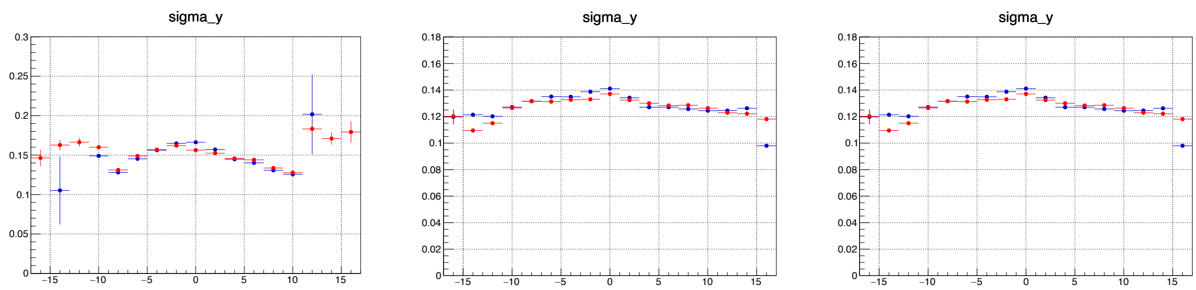

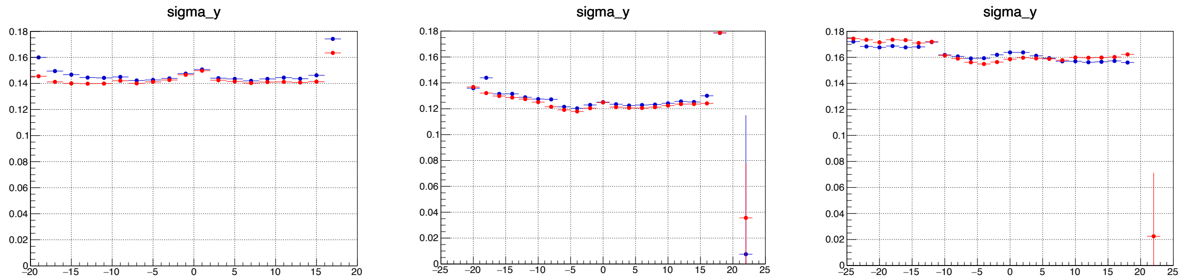

Figure 12. The errors width comparison of the dy-residuals determination vs. y for all GEM station. Blue points - MC, red points - data. Reaction C + Cu, energy 4.0 GeV.

3. Residuals width vs. momentum corrections

The dependence of the dx-value versus momentum of track for each GEM was calculated. From the fit function (1.1) the distribution of the parameter p_5 value (width of the Gaussian function) depending on the momentum of track for each GEM station was calculated for data and MC (Fig. 13).

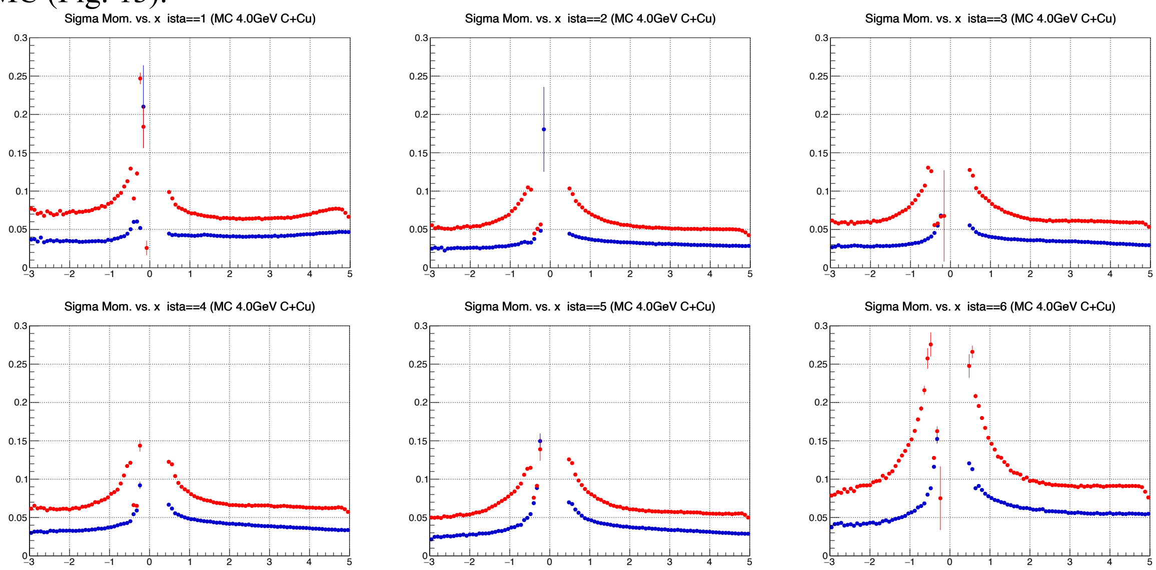

Figure 13. Dependencies residuals errors vs. track momentum for all GEM stations. Blue points - MC, red points - data. Reaction C + Cu, energy 4.0 GeV.

Using smearing function $\sigma_{smear} = \sqrt{\sigma_{data}^2 - \sigma_{MC}^2}$ residuals errors vs. track momentum distributions in MC were adjusted to the data (Fig. 14).

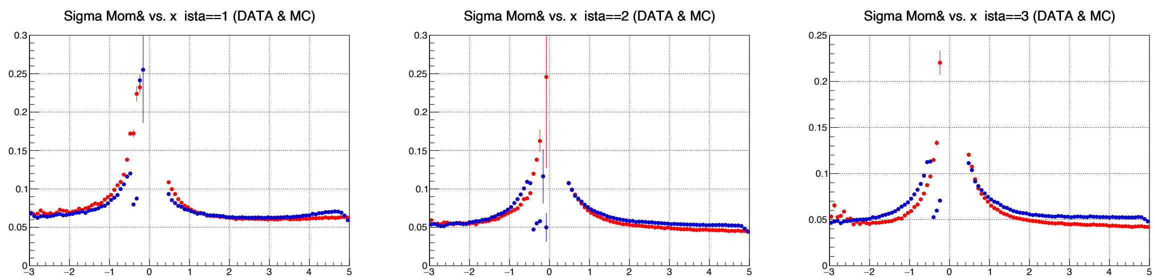

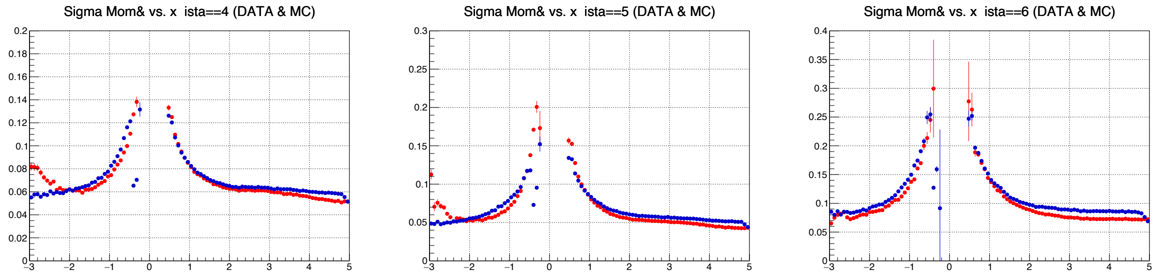

Figure 14. Dependencies residuals errors vs. track momentum for all GEM stations after smearing procedure. Blue points - MC, red points - data. Reaction *C+Cu*, energy 4.0 GeV.

Λ hyperon selection criteria

Λ-hyperon is a long living particle ($\tau = (2.632 \pm 0.020) \times 10^{-10} s$) which is decaying with the highest probability into two channels: Λ → pπ- with $BR = (63.9 \pm 0.5)\%$ and Λ → nπ0 with $BR = (35.9 \pm 0.5)\%$.

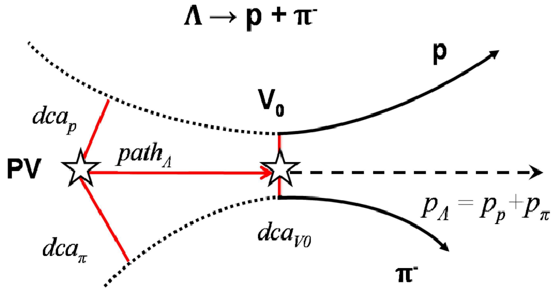

Figure. 15. Decay Scheme. Event topology: PV – primary vertex, V_0 – vertex of hyperon decay, dca – distance of the closest approach, path – decay length.

Λ hyperons were reconstructed using their decay mode into two oppositely-charged tracks Λ → pπ-. The signal event topology (decay of a relatively long-lived particle into two tracks) defined the selection criteria: small track-to-track separation in the decay vertex, relatively large decay length of the mother particle (Fig. 15).

After the track selection procedure, the next cuts were applied for the *Λ* hyperon signal selection:

1. Each track has at least 4 hits in Si and GEM detectors (7 detectors in total), where hit is a combination of two strip clusters on both readout sides (*X* and *X′* views) on each detector [1];
2. Momentum range of positive tracks: p_{pos}< 3.9, 4.4 GeV/*c* for 4.0 and 4.5 AGeV respectively;
3. Momentum range of negative tracks: p_{neg}> 0.3 GeV/*c*;
4. Distance of the closest approach of *V0* decay tracks (distance in X-Y plane between *V0* decay tracks at Z=Z_{V0}): *dca* < 1.0 cm;
5. Distance between *V0* and primary vertex: *path* > 2.5 cm.

Data and Monte-Carlo comparison

To evaluate the *Λ* hyperon acceptance and reconstruction efficiencies, minimum bias interactions of 4.0 and 4.5A GeV carbon beam with *C, Al, Cu, Pb* targets were generated with the DCM-QGSM generator. Distributions of the experimental primary vertex are given in Fig.16. The generated particles were traced through the BM@N geometry using the GEANT4 simulation and reconstructed using the BmnRoot software framework. The total number of MC generated events for each target and energy is ~3.8x10^7.

Experimental and Monte-Carlo distributions of the number of tracks reconstructed in the primary vertex and number of hits per track for positive and negative are presented in Fig.17 and Fig.18 for 4.0 and 4.5 AGeV carbon beam data, respectively. Distributions of the transverse momentum p_T and total momentum p of reconstructed positive and negative particles in data and MC simulation are shown in Fig.19 and Fig.20 for interactions of 4.0 and 4.5 AGeV carbon beam, respectively. Distributions of spatial parameters used for the Λ hyperon selection are presented in Fig.21 and Fig. 22. for 4.0 and 4.5 AGeV energies respectively.

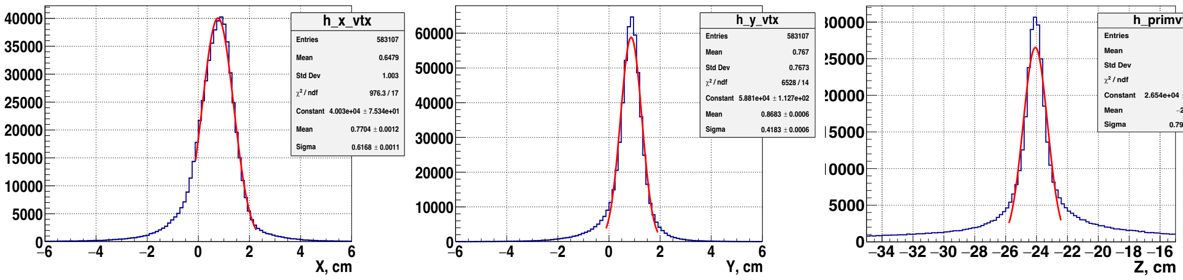

Figure. 16. *X,Y,Z* distributions of the experimental primary vertex

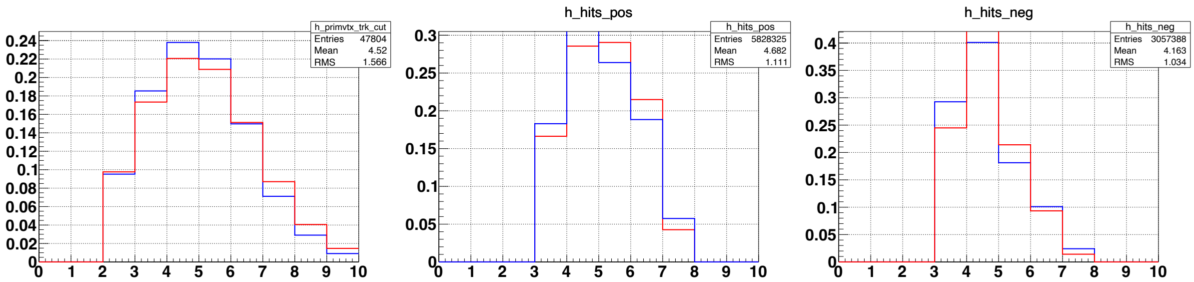

Figure. 17. *C+Cu* interactions at 4.0 AGeV carbon beam energy: number of tracks reconstructed in the primary vertex (left); number of hits per reconstructed track for positive particle (center); number of hits per reconstructed track for negative particle (right). Blue points - MC, red points - data.

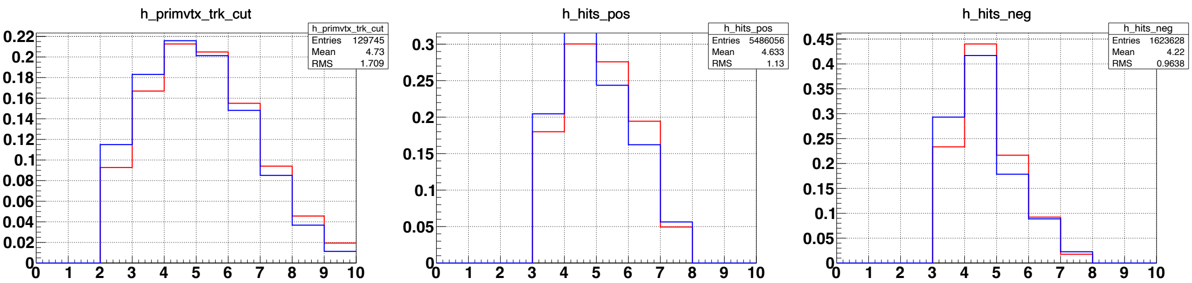

Figure. 18. *C+Cu* interactions at 4.5 AGeV carbon beam energy: number of tracks reconstructed in the primary vertex (left); number of hits per reconstructed track for positive particle (center); number of hits per reconstructed track for negative particle (right). Blue points - MC, red points - data.

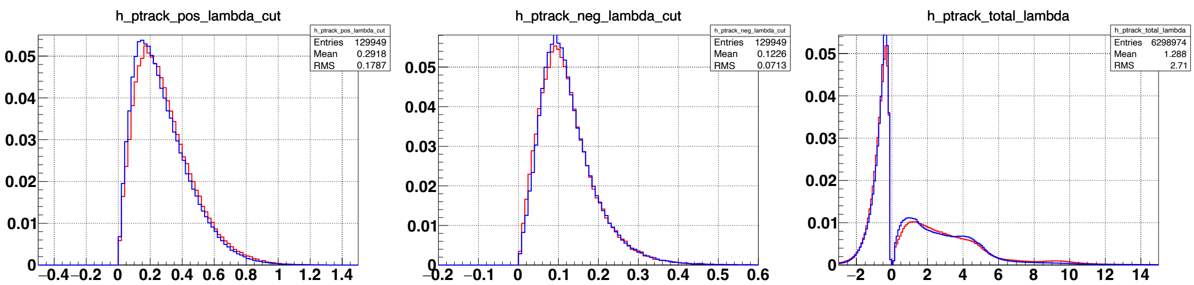

Figure 19. *C+Cu* interactions at 4.0 AGeV carbon beam energy: transverse momentum of positive particles (left); transverse momentum of negative particles (center); total momentum of negative (*p/q*<0) and positive particles (*p/q*>0) (right). Blue points - MC, red points - data.

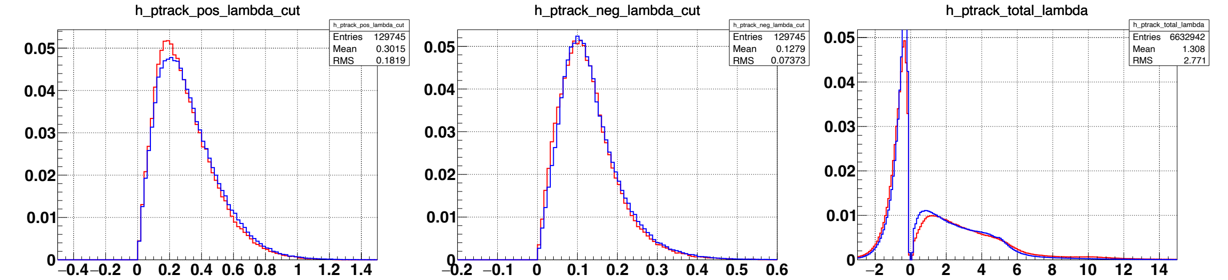

Figure 20. *C+Cu* interactions at 4.5 AGeV carbon beam energy: transverse momentum of positive particles (left); transverse momentum of negative particles (center); total momentum of negative (*p/q*<0) and positive particles (*p/q*>0) (right). Blue points - MC, red points - data.

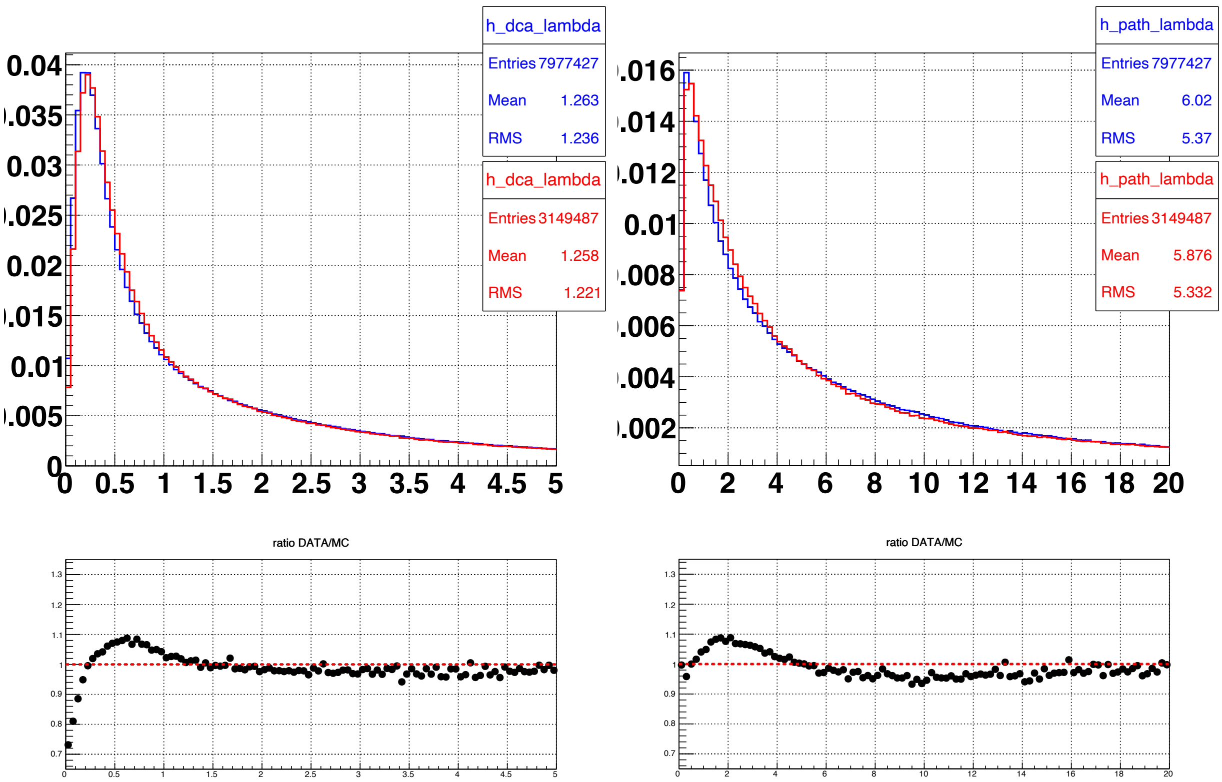

Figure 21. Distance of the closest approach of *V0* decay tracks (*dca*), distance between the primary vertex and *V0* (path). Ratio of the data/MC presented on bottom pictures. Cuts were applied as follow: dca<1.0, path>2.5. Reaction *C+Cu*, energy 4.0 GeV.

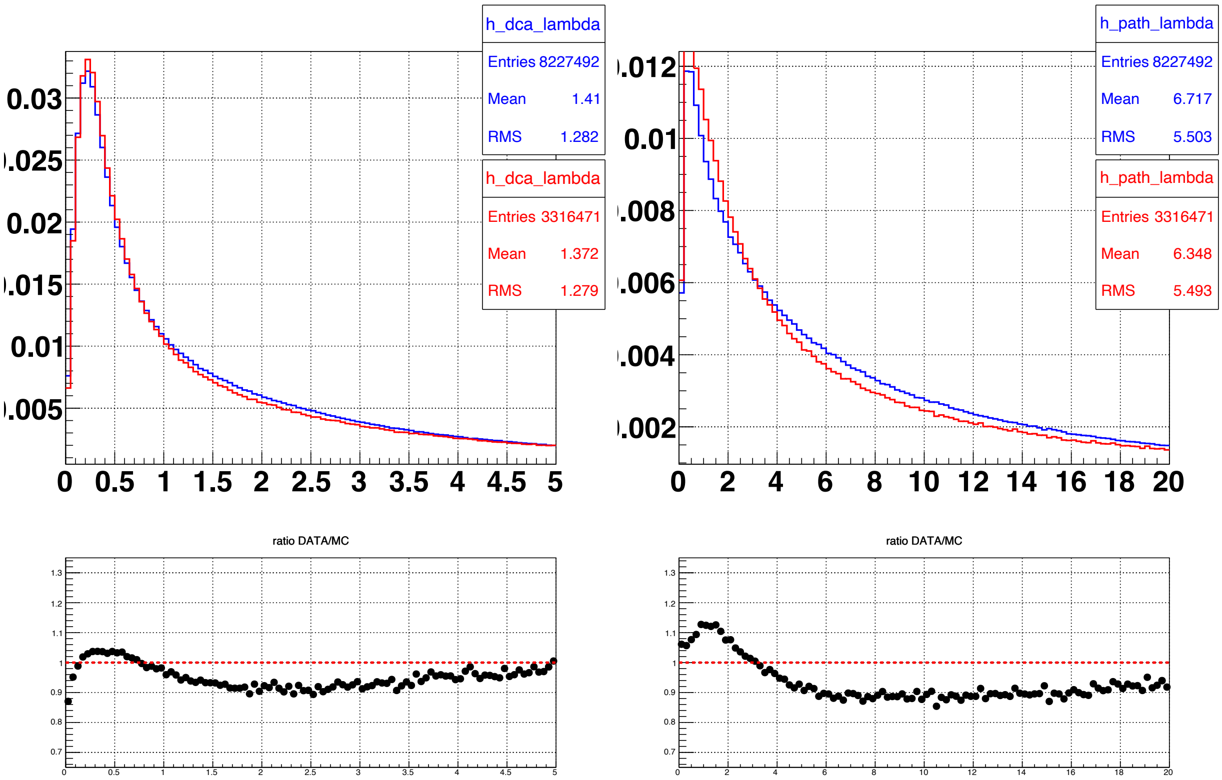

Figure 22. Distance of the closest approach of *V0* decay tracks (*dca*), distance between the primary vertex and *V0* (path). Ratio of the data/MC presented on bottom pictures. Cuts were applied as follow: dca<1.0, path>2.5. Reaction *C+Cu*, energy 4.5 GeV.

Trigger efficiency

The trigger efficiency ε_{trig} calculated for events with reconstructed Λ hyperons in interactions of carbon beam with different targets is given in Table 3. The trigger efficiency was evaluated by a convolution of the MC simulation of the trigger BD detector response with reconstructed Λ hyperons and the GEANT4 MC simulation of delta electrons produced by the carbon beam in the *C, Al, Cu, Pb* targets which were found to be the dominant source of delta electrons. The dependence of the trigger efficiency on the collision impact parameter is presented in Fig.23 for interactions of the carbon beam with the *C, Al, Cu, Pb* targets.

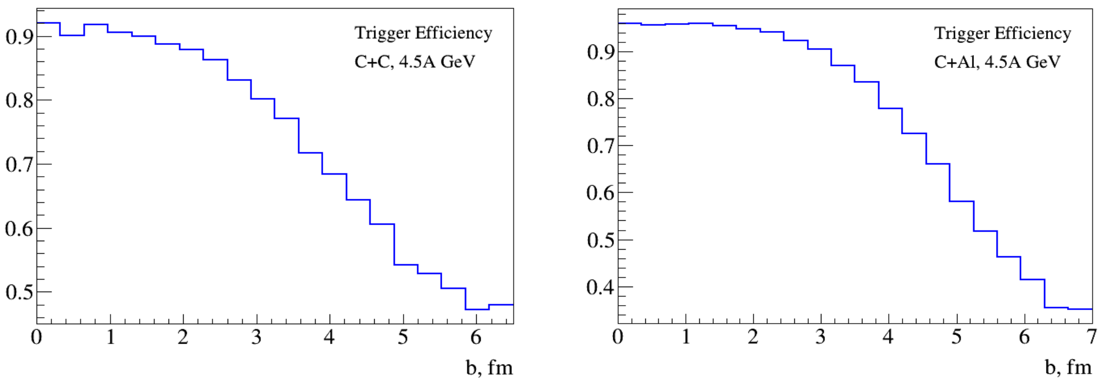

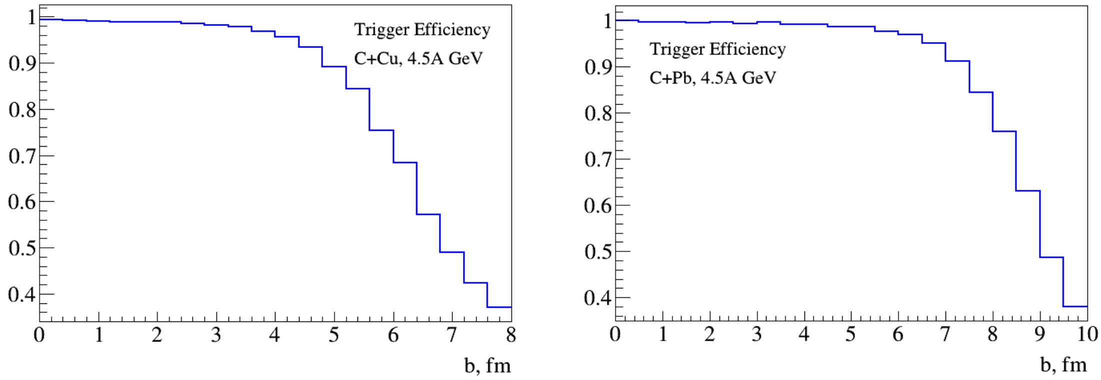

Figure 23. Trigger efficiency (ε_{trig}) as a function of the collision impact parameter. Distributions was obtained for MC events of the carbon beam with the *C, Al, Cu, Pb* targets at 4.5 AGeV.

Table 3. Trigger efficiency estimated with reconstructed *Λ* hyperons in interactions of the carbon beam with *C, Al, Cu, Pb* targets.

Trigger / Target 4.0 AGeV	***C***	***Al***	***Cu***	***Pb***
ε_{trig} (BD>=2)	0.80±0.02			
ε_{trig} (BD>=3)		0.87±0.02	0.92±0.02	0.95±0.02

Trigger / Target 4.5 AGeV	***C***	***Al***	***Cu***	***Pb***
ε_{trig} (BD>=2)	0.80±0.02			
ε_{trig} (BD>=3)		0.83±0.02	0.91±0.02	0.94±0.02

The systematic errors in Table 3 cover:

1. the contribution of delta electrons background produced in the simulated targets with the fractional thickness from 0.5 to 1 of the real targets;
2. the spread of the trigger efficiency values calculated for different y and p_T bins of reconstructed *Λ* hyperons;
3. change in the trigger efficiency after adjustment (reweighting) of the simulated track multiplicity to the experimental distributions.

The trigger efficiency obtained in simulation was cross checked by the analysis of data samples with the reduced trigger requirements: BD>=1 for *C+C* interactions and BD>=2 for *C+Al* and *C+Cu* interactions. The evaluated efficiencies for events with reconstructed *Λ* ε(BD>=2)/ε(BD>=1, *C+C*) = 0.90, ε(BD>=3)/ε(BD>=2, *C+Al*, *C+Cu, C+Pb*) = 0.95 are consistent with the same ratios of the trigger efficiencies calculated using simulated events.

Impact parameter distribution

Distributions of the impact parameters of minimum bias interactions generated with the DCM-QGSM, UrQMD and PSHD models are shown in Fig. 24. The impact parameter distributions of generated events with *Λ* hyperons as well as the impact parameters of simulated events with reconstructed *Λ* hyperons are presented for comparison. The *Λ* reconstruction requirements and the trigger conditions do not change much the impact parameter distributions. The mean values of the impact parameters for events with *Λ* hyperons generated in *C+C, C+Al, C+Cu, C+Pb* interactions by the DCM-QGSM model are presented in Table 4.

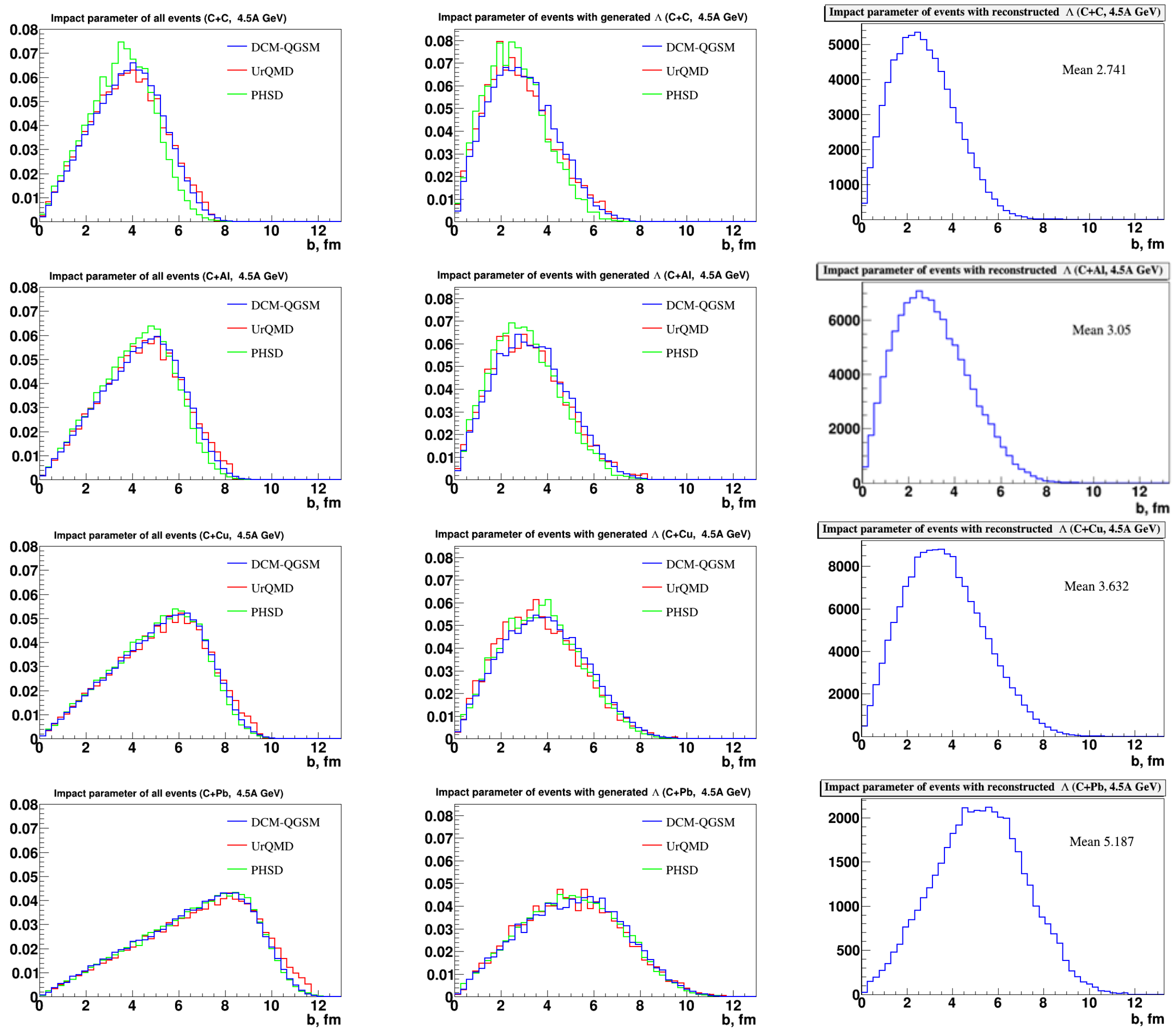

Figure 24. Impact parameter distributions of minimum bias interactions of 4.5 AGeV carbon beam with *C, Al, Cu, Pb* targets for the DCM-QGSM, UrQMD and PHSD models: all generated events (left), generated *Λ* hyperons (center), reconstructed *Λ* hyperons (right).

Table 4. Mean impact parameters of min. bias *C+C, C+Al, C+Cu* and *C+Pb* interactions generated by the DCM-QGSM model.

MC	*b*, fm (*C+C*)	*b*, fm (*C+Al*)	*b*, fm (*C+Cu*)	*b*, fm (*C+Pb*)
All min bias events	3.76	4.36	5.13	6.6
Events with *Λ*	2.80	3.08	3.58	4.8
Events with rec. *Λ*	2.71	3.18	3.88	5.2

Λ reconstruction efficiency [7]

The *Λ* reconstruction efficiency is the ratio of the number of reconstructed *Λ* hyperons to the number of generated ones in the intervals of (y, p_T), where y is measured in the laboratory frame. The kinematic ranges for (y, p_T) are $1.2 < y < 2.1$, $0.10 < p_T < 1.05\ GeV/c$.

The reconstruction efficiency was obtained as following. The kinematic range was divided into 8×8 cells for simulated and reconstructed MC data (Fig. 25 left plots). In each *i*-cell, the total number of simulated *Λ*-hyperons was calculated (N_{gen_i}).

For reconstructed MC events the invariant mass distributions were calculated using the pair combinations of the protons and negative pions for each cell. The total number of reconstructed *Λ*-hyperons was extracted from the obtained invariant mass distributions. The fit function for the background estimation is presented in (1.3). *Λ*-hyperons signal peak region 1.1075-1.125 GeV/c^2 was excluded from the fit procedure.

Number of the reconstructed Λ-hyperons N_{rec_i} (signal) was calculated as difference between all events in the signal peak region and events obtained under fit function shape (background) (Fig. 25 right plots). The background was determined in the 1.1075-1.125 GeV/c^2 mass range window.

$$f_b = N \cdot (x - M_0)^A \cdot e^{-B \cdot (x - M_0)} \quad (1.3)$$

where N, A , B – free parameters of the fit function;
$M_0 = 1.078\ GeV/c^2$ – invariant mass of the Λ;
x – mass of the (p, π$^-$) reconstructed pair.

The ratio of the reconstructed Λ-hyperons to the total number of generated Λ-hyperons gives the reconstruction efficiency:

$$\omega_i = N_{rec\_i} / N_{gen\_i} \quad (1.4)$$

The distributions of the Λ-hyperon signal reconstruction efficiency in the considerate *(y, p_T)* kinematic region are shown in Fig. 26 and Fig. 27 for 4.0 GeV and 4.5 AGeV beam kinetic energy respectively. Kinematic cells with efficiency $\omega_i < 0.01$ were excluded from the analysis. They are shown in white in Figures 26-27. For the reconstruction efficiency correction in cells with $\omega_i < 0.01$ the extrapolation factors value (f$_{extrap}$) were calculated using DCM-QGSM model.

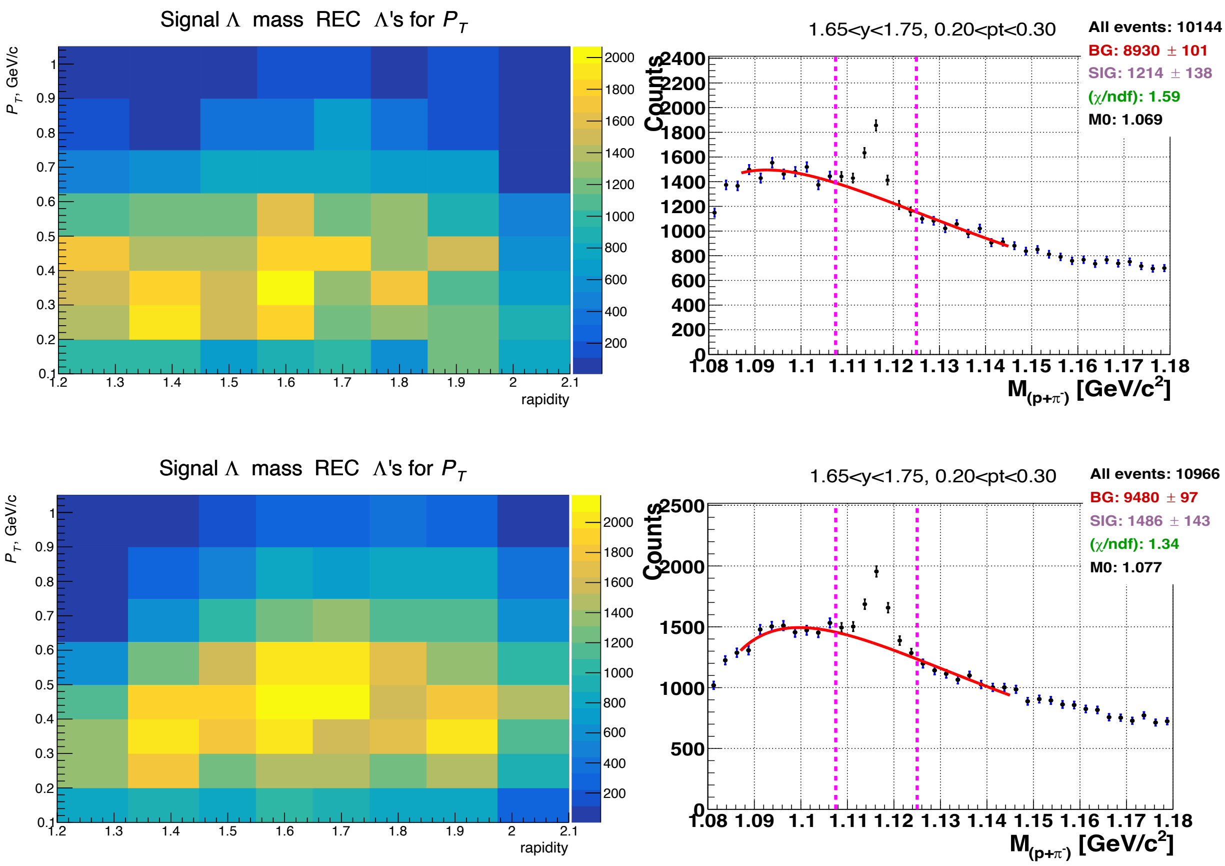

Figure 25. *C+Cu* reaction. The MC distribution of the reconstructed signal in full acceptance with beam energy 4.0AGeV (top left) and 4.5AGeV (bottom left). The mass distribution and background fit in kinematic range $0.20 < p_T < 0.30\ GeV/c$, 1.65 < *y* <1.75 for 4.0AGeV (top right) and 4.5AGeV (bottom right). The red line is the fit function (1.3).

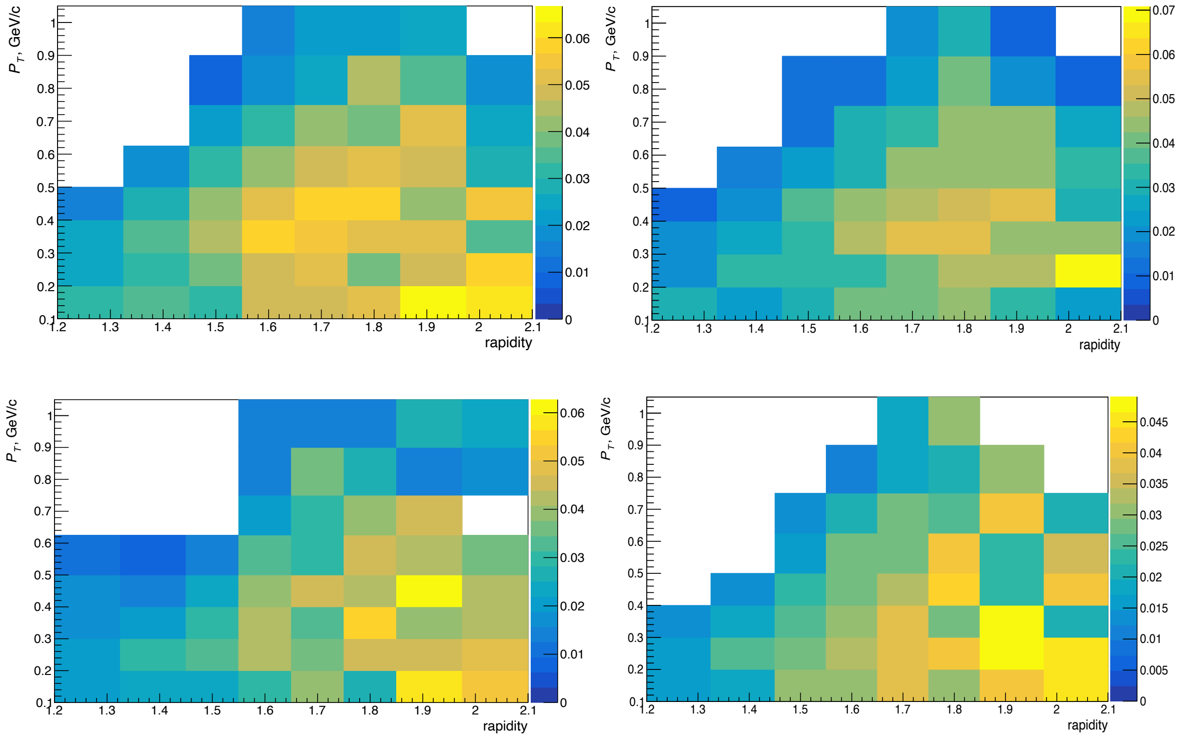

Figure 26. The MC distribution of *Λ* reconstruction efficiency in (*y,pT*) bins for 4.0 AGeV energy: *C+C* interactions (top left); *C+Al* interactions(top right); *C+Cu* interactions (bottom left); *C+Pb* interactions (bottom right).

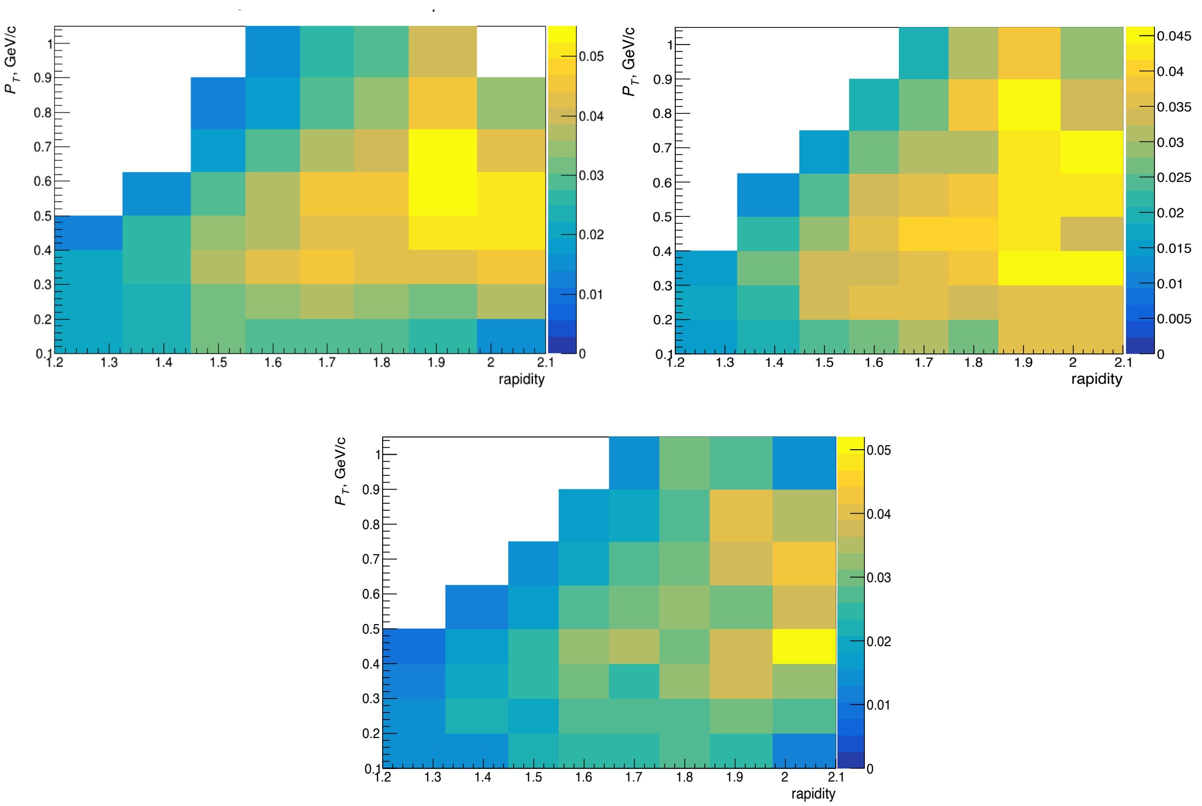

Figure 27. The MC distribution of *Λ* reconstruction efficiency in (*y,pT*) bins for 4.5 AGeV energy: *C+C* interactions (top left); *C+Al* interactions(top right); *C+Cu* interactions (bottom).

The extrapolation factor f_{extrap} was calculated as a ratio of the number of all MC generated *Λ*-hyperons in cell column along p_T to the number of MC reconstructed *Λ*-hyperons with the reconstruction efficiency above $\omega_i > 0.01$ in this column. The extrapolation factor is determined using the formula:

$$\mathrm{f}_{extrap} = {N_{all\_gen}}/{N_{cons}} \tag{1.5}$$

where: $\mathrm{N}_{\mathrm{all\_gen}}$ - is the sum of all generated events in cell column along p_T;

N_{cons} - is the sum of reconstructed events with $\omega_i \geq 0.01$ in the considered cell column along p_T;

Due the low statistics in the physical data for the *Λ* cross sections and yield values calculations the obtained MC extrapolation factors were summed into 4×4 cells matrix in the (*y*, p_T) kinematic range. The extrapolation factor for the efficiency corrections for cells with $\omega_i < 0.01$ was determined for each *C+A* reaction separately. They are presented in Table 5.

Table 5. The values of the MC generated *Λ*-hyperons, number of the reconstructed MC *Λ*-hyperons and calculated extrapolation factors.

***y* range**	**Tkin = 4.0 AGeV**		
	C+C		
1.20 - 1.45	712131	409932	1.74 ± 0.003
1.45 - 1.65	497063	455375	1.09 ± 0.002
1.85 - 2.10	245509	243472	1.01 ± 0.003
	C+Al		
1.20 - 1.45	930423	538999	1.73 ± 0.003
1.45 - 1.65	594258	562752	1.06 ± 0.002
1.85 - 2.10	257086	255172	1.01 ± 0.003
	C+Cu		
1.20 - 1.45	1088598	730706	1.49 ± 0.002
1.45 - 1.65	634805	531683	1.19 ± 0.002
1.85 - 2.10	239136	229466	1.04 ± 0.003
	C+Pb		
1.20 - 1.45	992297	415147	2.40 ± 0.004
1.45 - 1.65	518536	458611	1.13 ± 0.002
1.85 - 2.10	176170	171242	1.03 ± 0.003

***y* range**	**Tkin = 4.5 AGeV**		
	C+C		
1.20 - 1.45	956603	441817	2.17±0.004
1.45 - 1.65	723551	695781	1.04±0.002
1.85 - 2.10	452888	447921	1.01±0.002
	C+Al		
1.20 - 1.45	1271777	611399	2.08 ± 0.003
1.45 - 1.65	881912	764628	1.15 ± 0.002
	C+Cu		
1.20 - 1.45	1538870	739101	2.08 ± 0.003
1.45 - 1.65	967469	840427	1.15 ± 0.002

Λ hyperon signal in data

The signal from *Λ*-hyperon decays is observed as a narrow peak in the invariant mass distribution of the two tracks with opposite charge with the proton and pion mass hypothesis. The detector acceptance, momentum, angular resolution, and the primary vertex reconstruction set the constraints for the analysis of $C+A$ data. This provides instruments for background separation.

For each event in the experimental data, the weight ω_i equal to the reconstruction efficiency in the (y, p_T) bin (see 1.4), was assigned, according to corresponding kinematic cell this event belongs. The invariant mass distribution for weighted data events was calculated for each cell with a weight of $1/\omega_i$. The cell contents were summed separately by column $\sum_{ij} pT_{ij}$ and by row $\sum_{ij} y_{ij}$, respectively.

For the background estimation, the mass distributions were fitted with the 4th order (1.6) polynomial function. The fits ranges were chosen according to the best ratio of the $\chi^2/ndf \sim 1$. The mass window for Λ signal extraction was set within 1.1075-1.125 GeV/c^2 range and was excluded from the background polynomial fit.

of the background distribution fit range was chosen according to the best

The numbers of Λ hyperons were determined from the content of the background-subtracted histogram bins within mass window.

$$F\left(M_{p\pi^-}\right)_{bg} = p_0 + p_1 M_{p\pi^-} + p_2 M_{p\pi^-}{}^2 + p_3 M_{p\pi^-}{}^3 + p_4 M_{p\pi^-}{}^4 \qquad (1.6)$$

where: $p_0, \ldots p_4$ are free parameters of the fit function;
$M_{p\pi^-}$ the mass value of the (p, π^-) pair.

Spectra of the invariant mass of (p, π^-) for weighted events reconstructed in interactions of 4.0 and 4.5 AGeV carbon beam with the superimposed background fit for the different targets are shown in Fig. 28 and 29, respectively. To obtain the Λ signal peak position and its width value the invariant mass ($M_{p\pi^-}$) distributions of the reconstructed (p, π^-) pairs were fitted using the sum of the functions 1.6 and 1.7: $F\left(M_{p\pi^-}\right)_{bg} + F\left(M_{p\pi^-}\right)_{signal}$.

$$F\left(M_{p\pi^-}\right)_{signal} = p_5 \exp\left(-\frac{1}{2}\left(\frac{\langle M_{p\pi^-}\rangle - p_6}{p_7}\right)^2\right) \qquad (1.7)$$

where: p_5 - free parameter of the fit function;
p_6 - the peak position of the Gaussian function;
p_7 - the width of the Gaussian function (the signal width);
$\langle M_{p\pi^-} \rangle$ - mass of the (p, π^-) reconstructed pair;

The shape of this fit function and extracted parameters are presented on Fig 28-29 in magenta color. Mass distribution was obtained in kinematic range $0.10 < p_T < 1.05\ GeV/$c, 1.2 < y <2.1. The value of the signal width varies in the range $\sigma_{Minv} \sim 2.0 - 4$ MeV/c^2 depending on the target. This variation in signal width values is due to the low statistics. Λ signals in intervals of the transverse momentum p_T and rapidity y were reconstructed using similar fit procedure as described above.

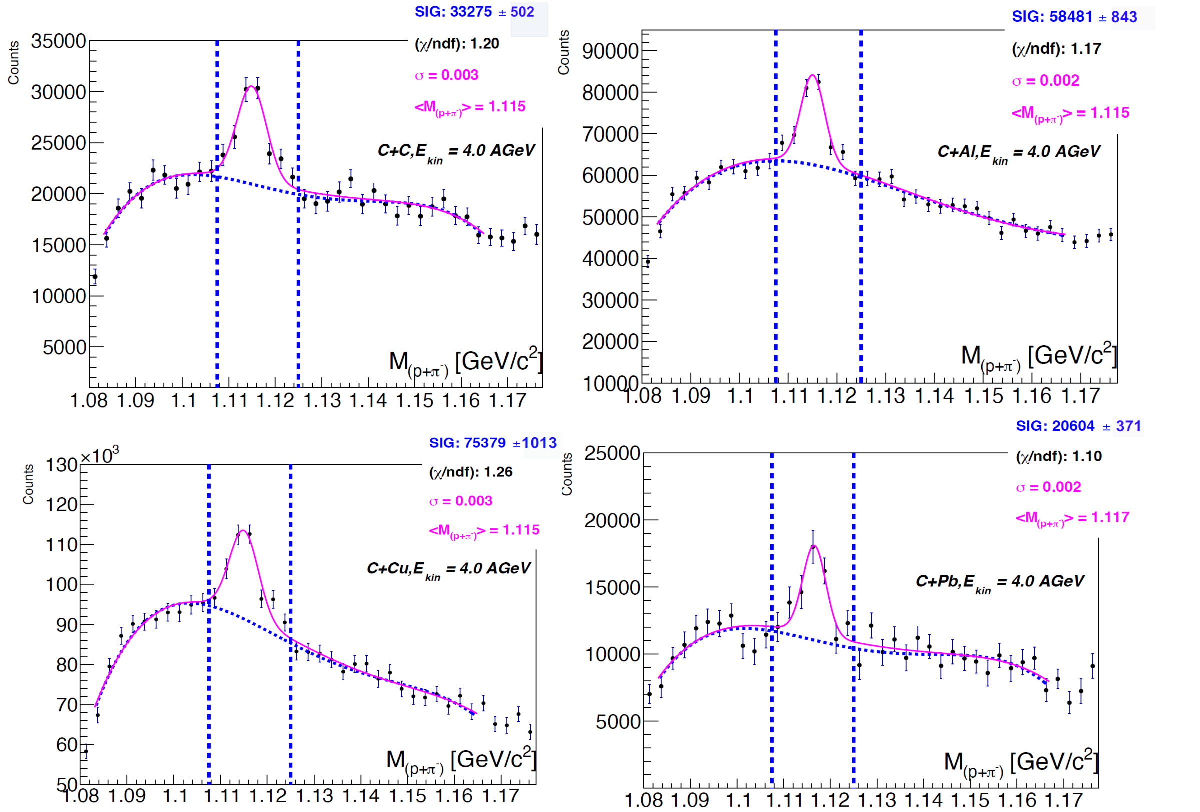

Figure 28. $\Lambda \rightarrow p\pi^-$ signal reconstructed in *C+C* (top left*), Al*(top right)*, Cu*(bottom left)*, Pb*(bottom right) interactions at 4.0 AGeV carbon beam energy. The background is fitted by the 4th degree polynomial function (blue dashed) and subtracted from the histogram content in the Λ signal mass range indicated by the vertical lines.

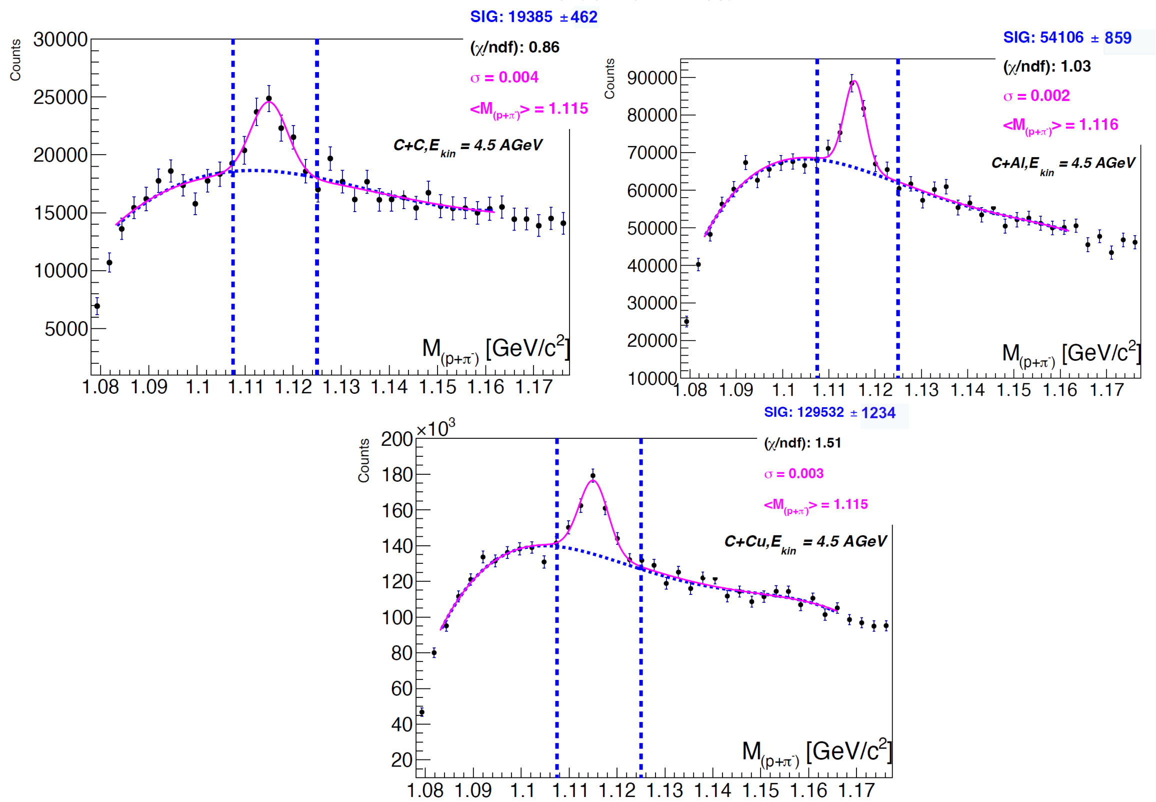

Figure 29. $\Lambda \rightarrow p\pi^-$ signal reconstructed in *C+C* (top left*), Al* (top right)*, Cu* (bottom)*,* interactions at 4.5 AGeV carbon beam energy. The background is fitted by the 4th degree polynomial function (blue dashed) and subtracted from the histogram content in the Λ signal mass range indicated by the vertical lines. Due the low statistics in the physical data the *C+Pb* process at 4.5AGeV was excluded from the analysis.

The statistical errors of the reconstructed signals were calculated using formula (1.8):

$$Err_{stat} = \sqrt{0.5 \times N_{bg\_events} + N_{mass\_events}} \tag{1.8}$$

where: N_{bg_events} - number of the estimated background events in the *Λ* mass window;
N_{mass_events} - total number of the events in the *Λ* mass window;

For the *Λ* reconstructed signal systematic errors estimation the physical data sets were divided into periods for each target and energy (periodI and periodII). For each period the $M_{p\pi^-}$ mass distributions were obtained and the number of background and signal events were calculated as described above. The $Err_{syst\_periods}$ value was determinate as:

$$Err_{syst\_periods} = \frac{|N_{rec\_perI} - N_{rec\_perII}|}{2 \times (N_{rec\_perI} + N_{rec\_perII}) \times \sqrt{2}} \tag{1.9}$$

where: N_{rec_perI} – number of signal events calculated in the periodI;
N_{rec_perII} – number of signal events calculated in the periodII;

Also, for systematic uncertainties study the $M_{p\pi^-}$ distributions spectra were fitted using function 1.3 for the full data sets. The reconstructed *Λ* signal values were extracted within mass window 1.1075-1.125 GeV/c^2. For this case the systematic errors were calculated with formula (1.10)

$$Err_{syst\_fitfun} = \frac{|N_{rec\_fit1} - N_{rec\_fit2}|}{N_{rec\_fit1}} \tag{1.10}$$

where: N_{rec_fit1} - number of calculated signal events using background fit function (1.7);
N_{rec_fit1} - number of calculated signal events using background fit function (1.3);

The total systematic error for the *Λ* reconstructed signal was determinated as:

$$Err_{syst\_tot} = \sqrt{Err^2_{syst\_periods} + Err^2_{syst\_fitfun}} \tag{1.11}$$

The statistics of *Λ* hyperons reconstructed in *C+C, C+Al, C+Cu, C+Pb* interactions in bins of *y* and p_T are summarized in Tables 6 and 7 for 4.0 AGeV and 4.5 AGeV carbon beam data, respectively.

Table 6. Reconstructed weighted signals of *Λ* hyperons in bins of *y* and p_T in 4.0 AGeV carbon-target interactions. The first error presents the statistical uncertainty, the second error is systematic.

Target / ***y* interval**	**C**	**Al**	**Cu**	**Pb**
1.2-1.45	10570±288±34	26638±495±39	23262±601±95	7273±229±40
1.45-1.65	9089±209±63	19061±384±31	17117±498±68	3637±173±59
1.65-1.85	8131±232±43	10176±371±90	15993±467±91	3598±163±29
1.85-2.1	5996±269±95	7317±421±88	13350±443±78	3539±165±44

Target / ***p_T* interval**	**C**	**Al**	**Cu**	**Pb**

0.1-0.3	7021±321±41	15089±527±79	17988±620±33	6749±260±42
0.3-0.5	8287±291±29	22919±493±58	19658±593±54	6030±202±28
0.5-0.85	8516±223±12	11893±361±30	12088±456±41	4898±161±87
0.85-1.05	1108±119±25	3683±242±40	8313±283±13	613±41±27

Table 7. Reconstructed weighted signals of Λ hyperons in bins of y and p_T in 4.5 AGeV carbon-target interactions. The first error presents the statistical uncertainty, the second error is systematic.

Target / y interval	C	Al	Cu	Pb
1.2-1.45	8597±275±63	16787 ± 574±81	49942±790±142	16366±640±46
1.45-1.65	4097±184±32	21632 ± 478±97	32603±535±91	13378±409±43
1.65-1.85	2461±200±29	8946 ± 374±64	22908±524±83	5957±383±20
1.85-2.1	5767±251±53	10735 ± 201±86	16531±576±53	2051±394±22

Target / p_T interval	C	Al	Cu	Pb
0.1-0.3	5164±313±62	13642±526±61	34956±814±140	12043±656±13
0.3-0.5	8859±259±44	19480±375±28	42945±715±131	12259±539±39
0.5-0.85	4085±185±24	12735±377±29	25972±521±92	11126±338±51
0.85-1.05	2176±116±27	4275±422±33	8765±289±73	3305±208±11

Evaluation of Λ hyperon cross sections and spectra:

The inclusive cross section σ_Λ and yield Y_Λ of Λ hyperon production in *C+C, C+Al, C+Cu, C+Pb* interactions are calculated in bins of y (p_T) according to the next formulas:

$$\sigma_\Lambda(y) = \sum_{p_T}\left(N_{rec}^{\Lambda}(y,p_T)/\varepsilon_{rec}(y,p_T)\right)/(\varepsilon_{trig} \times \varepsilon_{pileup} \times L) \quad (1.12)$$

$$\sigma_\Lambda(p_T) = \sum_{y}\left(N_{rec}^{\Lambda}(y,p_T)/\varepsilon_{rec}(y,p_T)\right)/(\varepsilon_{trig} \times \varepsilon_{pileup} \times L) \quad (1.13)$$

$$Y_\Lambda(y) = \sigma_\Lambda(y)/\sigma_{inel} \quad (1.14)$$

$$Y_\Lambda(p_T) = \sigma_\Lambda(p_T)/\sigma_{inel} \quad (1.15)$$

where: L is the luminosity (Table 2);

$N_{rec}{}^{\Lambda}/\ \varepsilon_{rec}$ - the number of reconstructed Λ hyperons, corrected to ε_{rec} – the combined efficiency of the Λ hyperon reconstruction (Tables 6 and 7);

ε_{trig} – the trigger efficiency (Table 3);

ε_{pileup} – the beam halo and pile-up suppression factor (Table 1),

σ_{inel}–the cross section for minimum bias inelastic *C+A* interactions (Table 8).

The cross section for inelastic C+C interactions is taken from the measurement [8]. The cross sections for inelastic *C+Al, C+Cu, C+Pb* interactions are taken from the predictions of the DCM-QGSM model which are consistent with the results calculated by the formula:

$$\sigma_{inel} = \pi R_0^2 (A_P^{\frac{1}{3}} + A_T^{\frac{1}{3}})^2 \quad (1.16)$$

where: R_0 = 1.2 fm is an effective nucleon radius,

A_P and A_T are atomic weight of the beam and target nucleus [9].

The uncertainties for *C+Al, C+Cu, C+Pb* inelastic cross sections are estimated by using the alternative formula:

$$\sigma_{inel} = \pi R_0^2 (A_P^{\frac{1}{3}} + A_T^{\frac{1}{3}} - b)^2 \qquad (1.17)$$

with R_0 = 1.46 fm and b = 1.21 [8].

Table 8. Inelastic cross sections for carbon-nucleus interactions.

Interaction	***C+C***	***C+Al***	***C+Cu***	***C+Pb***
Inelastic cross section, mb	830±50	1260±50	1790±50	3075±50

The yields of *Λ* hyperons in minimum bias *C+C, C+Al, C+Cu, C+Pb* interactions are measured in the kinematic range on the *Λ* transverse momentum of $0.1<p_T<1.05$ GeV/*c* and the *Λ* rapidity in the laboratory frame of $1.2<y<2.1$.

The rapidity of the beam-target nucleon-nucleon in center of mass (CM) system was calculated. The transformation of the *y* distribution to c.m.s. gives $y^*=y-y_{CM}$. The corrected differential *y** spectra of *Λ* hyperon yields are presented in Figs. 30 and 31 for 4.0 AGeV and 4.5 AGeV carbon beam energies, respectively. The differential p_T spectra of *Λ* hyperon yields are presented in Figs. 32 and 33. The predictions of the DCM-QGSM, URQMD and PHSD models were calculated and shown for comparison. Due the low statistics in the physical data the *C+Pb* process at 4.5AGeV was excluded from the analysis.

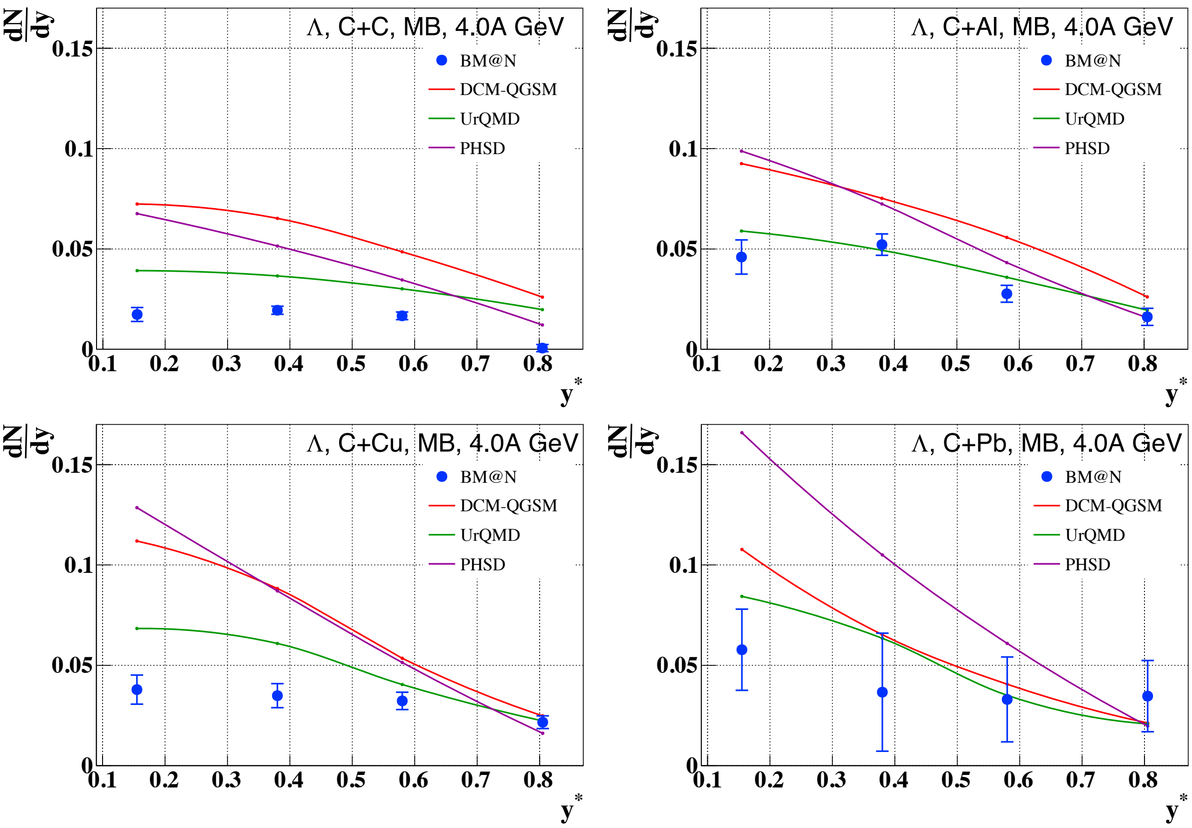

Figure 30. Reconstructed rapidity y* spectra of *Λ* hyperons in minimum bias *C+C, C+Al, C+Cu, C+Pb* interactions at 4.0 AGeV carbon beam energy (blue symbols, statistic error only). Predictions of the DCM-QGSM, UrQMD and PHSD models are shown as red, green and magenta lines.

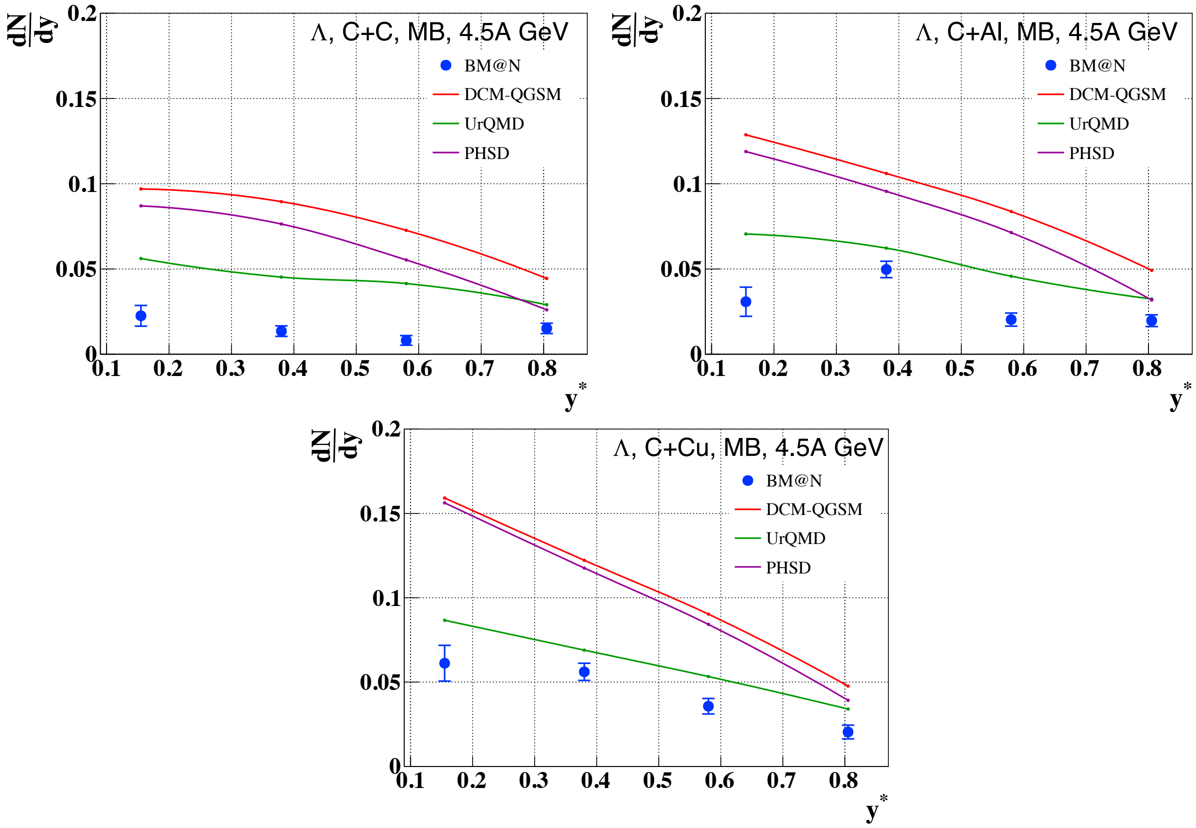

Figure 31. Reconstructed rapidity y* spectra of *Λ* hyperons in minimum bias *C+C, C+Al, C+Cu* interactions at 4.5 AGeV carbon beam energy (blue symbols, statistic error only). Predictions of the DCM-QGSM, UrQMD and PHSD models are shown as red, green and magenta lines.

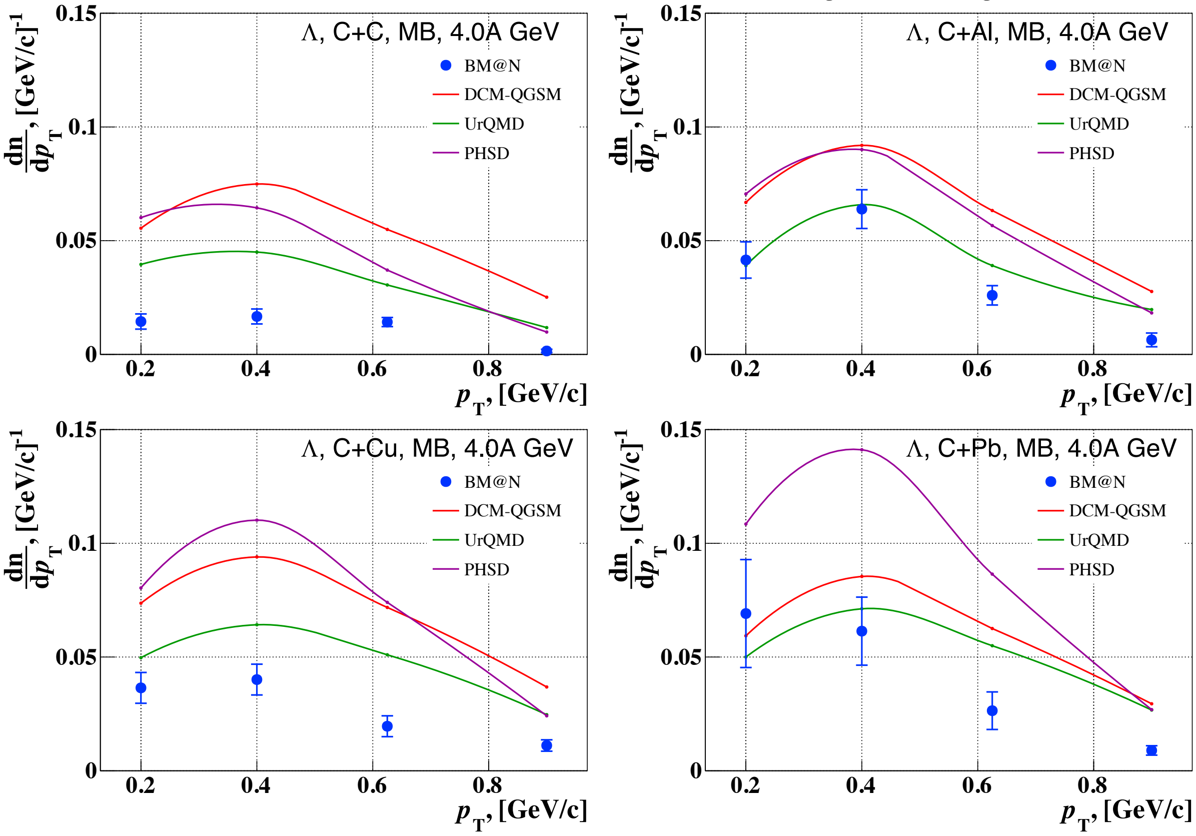

Figure 32. Reconstructed transverse momentum p_T spectra of *Λ* hyperons in minimum bias *C+C, C+Al, C+Cu, C+Pb* interactions at 4.0 AGeV carbon beam energy (blue symbols, statistic error only). Predictions of the DCM-QGSM, UrQMD and PHSD models are shown as red, green and magenta lines.

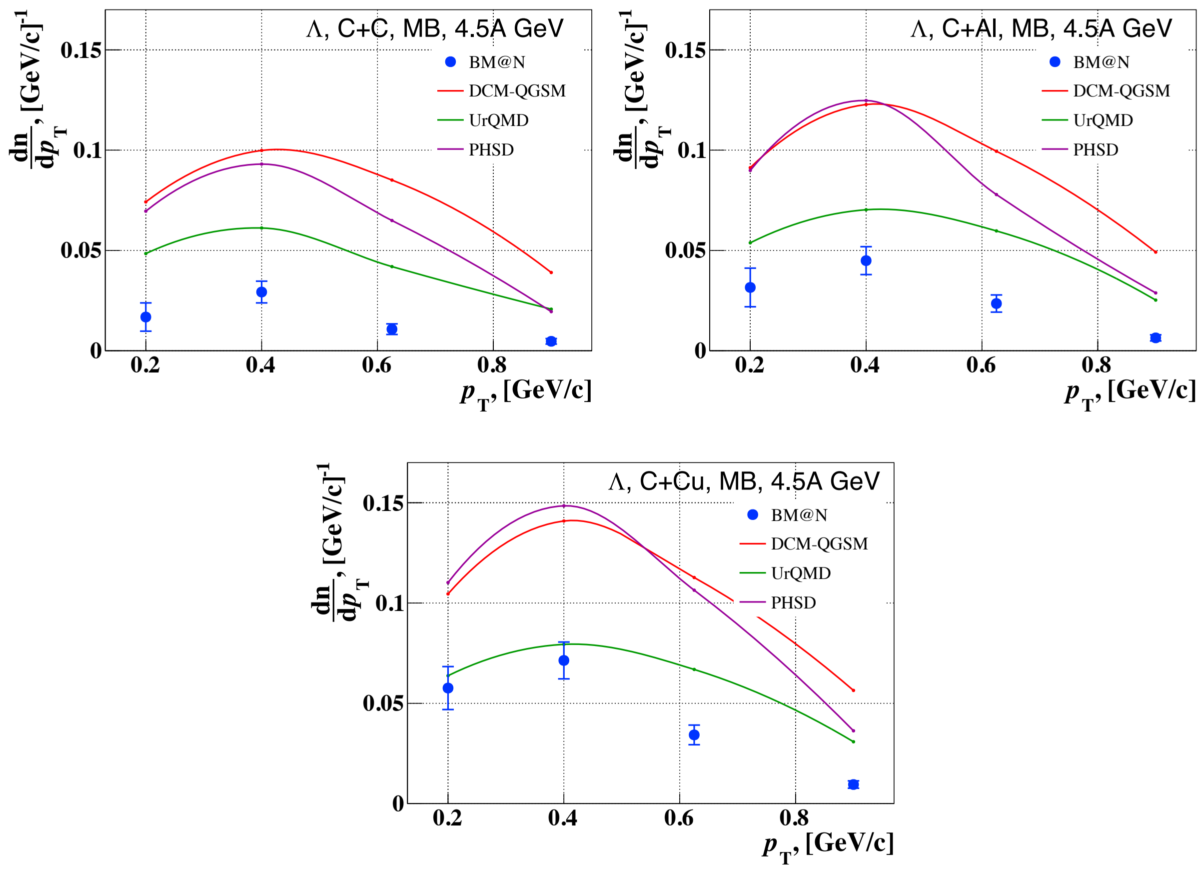

Figure 33. Reconstructed transverse momentum p_T spectra of Λ hyperons in minimum bias *C+C, C+Al, C+Cu* interactions at 4.5 AGeV carbon beam energy (blue symbols, statistic error only). Predictions of the DCM-QGSM, UrQMD and PHSD models are shown as red, green and magenta lines.

The measured differential spectra of the Λ yields in p_T region were parameterized by the form:

$$\frac{1}{p_T}\frac{d^2N}{dp_T dy} = N \times \exp\left(-\frac{m_T - m_\Lambda}{T_0}\right) \qquad (1.18)$$

where: $m_T = \sqrt{m_\Lambda^2 + p_T^2}$ - transverse mass;
N – normalization parameter;
T_0 – inverse slope parameter;
dy - corresponds to the measured y range.

T_0 parameter was estimated for the experimental Λ spectra and was compared with the predictions of the DCM-QGSM, URQMD and PHSD models Fig. 34 and Fig. 35 for the 4.0 AGeV and 4.5AGeV respectively. Due the low statistics and unstable fit the *C+Pb* process was excluded from the T_0 calculations for 4.5 AGeV energy. The values of the inverse slope T_0, extracted from the fit of the p_T spectra are summarized in Table 9. Calculations for the T_0 were also done for the periods for each target and energy (periodI and periodII).

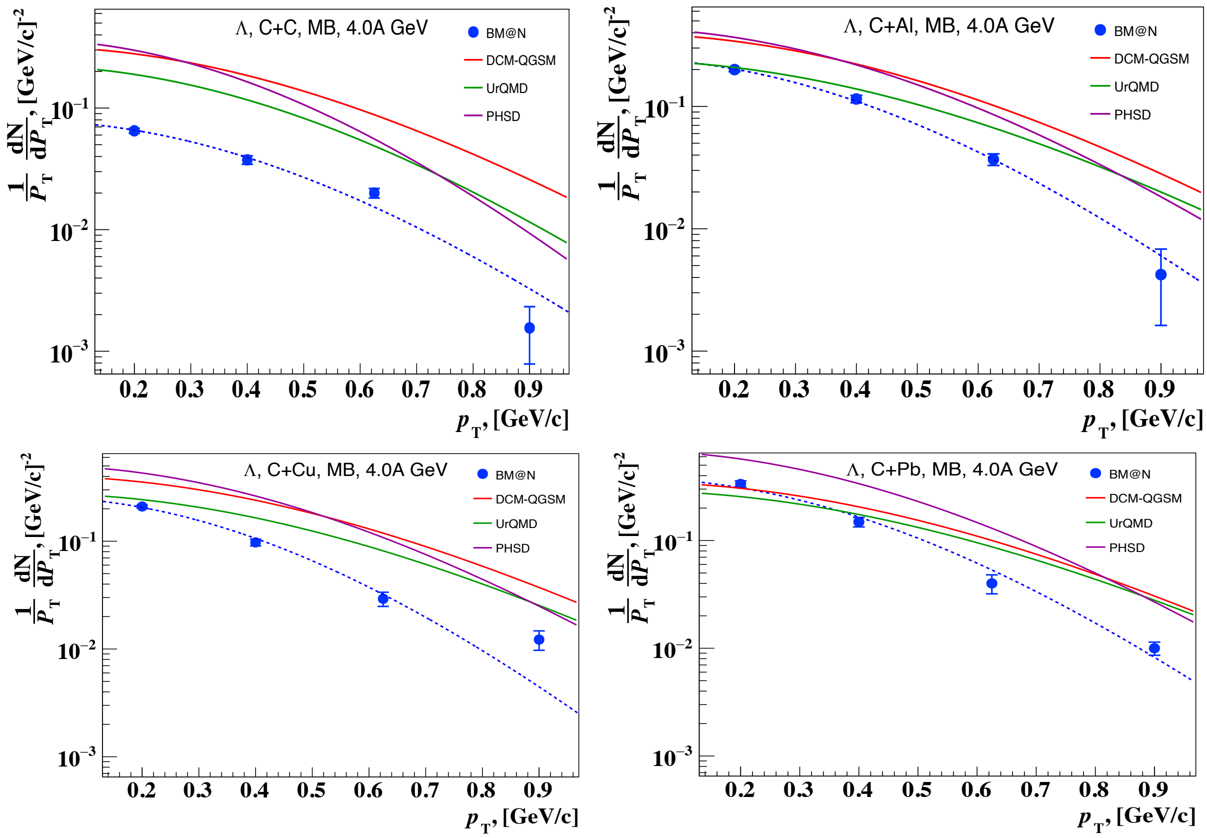

Figure 34. Invariant transverse momentum p_T spectra of Λ hyperons in minimum bias *C+C* (top left), *C+Al* (top right), *C+Cu* (bottom) interactions at 4.0 AGeV carbon beam energy (blue symbols, statistic error only). The error bars represent the statistical errors. Predictions of the DCM-QGSM, UrQMD and PHSD models are shown as red, green and magenta lines; the data fit are shown as blue dashed line.

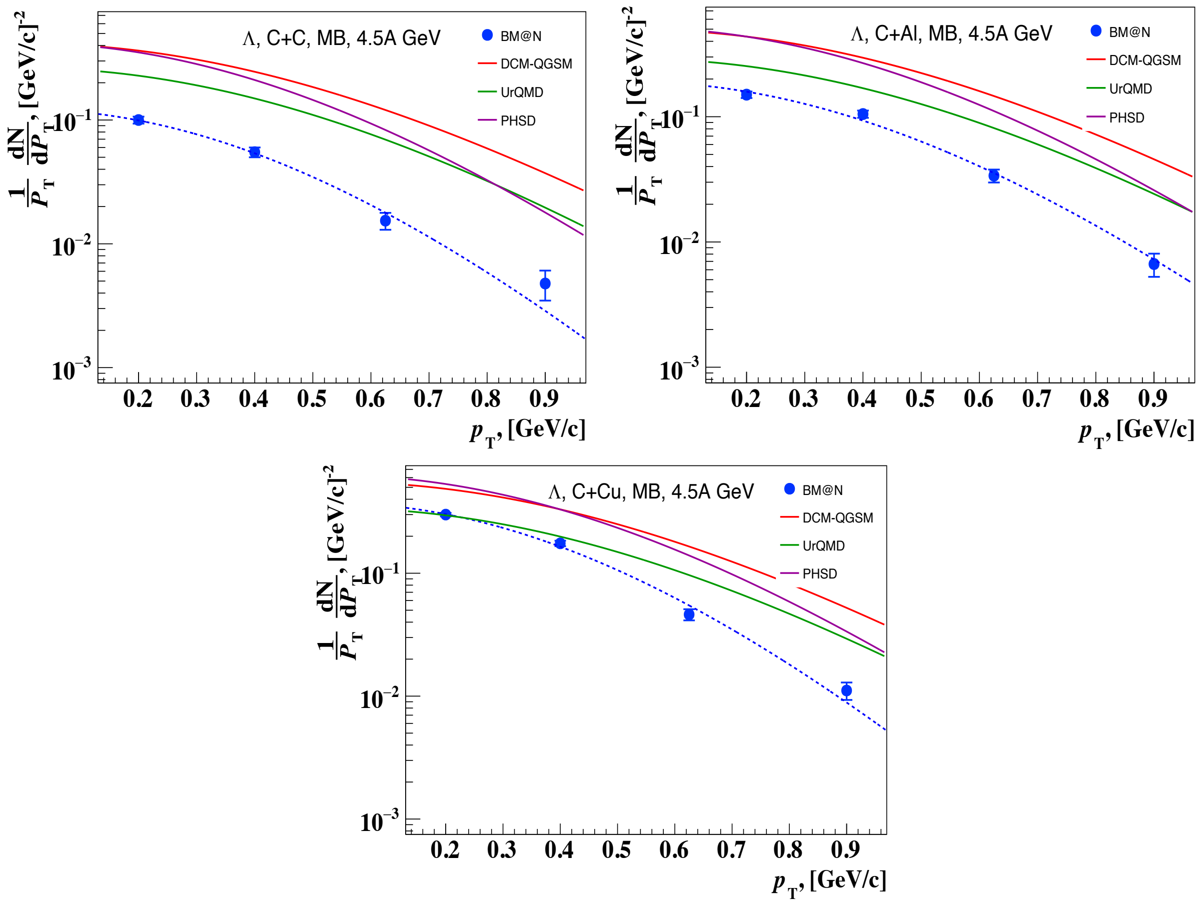

Figure 35. Invariant transverse momentum p_T spectra of Λ hyperons in minimum bias *C+C* (top left*),* *C+Al* (top right)*,* *C+Cu* (bottom left), *C+Pb* (bottom right) interactions at 4.5 AGeV carbon beam energy (blue symbols, statistic error only). The error bars represent the statistical errors. Predictions of the DCM-QGSM, UrQMD and PHSD models are shown as red, green and magenta lines.

Table 9. Inverse slope parameter extracted from the fit of the p_T spectra.

4.0 AGeV	***T_0*, MeV (*C+C*)**	***T_0*, MeV (*C+Al*)**	***T_0*, MeV (*C+Cu*)**	***T_0*, MeV *(C+Pb)***
BM@N	114 ± 19 ± 4	108 ± 16 ± 4	96 ± 14 ± 1	83± 8 ± 1
period I (T_1)	118±18	105±11	103±19	-
period II (T_2)	112 ±20	109±17	105±16	-
DCM-QGSM	126	120	133	130
UrQMD	107	128	133	136
PHSD	87	100	105	98

4.5 AGeV	***T_0*, MeV (*C+C*)**	***T_0*, MeV (*C+Al*)**	***T_0*, MeV (*C+Cu*)**	***T_0*, MeV *(C+Pb)***
BM@N	116 ± 24 ± 1	115 ± 7 ± 5	101 ± 3 ± 0,1	-
period I (T_1)	116±29	118±10	100±4	-
period II (T_2)	117±26	112±6	100±7	-
DCM-QGSM	132	133	135	142
UrQMD	122	128	130	134
PHSD	101	106	109	108

Systematic uncertainties

The systematic errors of the Λ in every p_T and y bin is calculated as difference between the obtained yields for the periodI and periodII for each target and energy (1.19).

$$Y_{syst\_per} = \left|Y_{per1} - Y_{per1}\right|/2 \qquad (1.19)$$

The global uncertainties from the Λ spatial parameters cuts variations accounts 5% for the *dca* (Fig. 21) and 5% for the fly distance (*path*) in the 4.0 AGeV energy dataset. For the 4.5 AGeV the numbers are 10% for the dca and 8% for the path (Fig 22). The final uncertainties were calculated as (1.20) and equals to the 7.1% and for the 4.0 AGeV, 12.2% for the 4.5 AGeV energy.

$$Y_{syst\_global} = \sqrt{dca^2_{syst.\ err} + path^2_{syst.\ err}} \qquad (1.20)$$

The Λ yield normalization uncertainty calculated as a quadratic sum of uncertainties of the trigger efficiency, luminosity and inelastic cross section.

The systematic uncertainties are summarized in Tables 10 and 11.

Table 10. Total systematic uncertainty of the Λ yield for 4.0 AGeV

Target / **Interval**	***y***				**Target** / **Interval**	***p_T***			
	C sys%	***Al*** sys%	***Cu*** sys%	*Pb* sys%		***C*** sys%	***Al*** sys%	***Cu*** sys%	***Pb*** sys%
1.2 -1.45	7.3	8.5	7.7	7.7	0.1 - 0.3	7.2	7.3	7.7	7.7
1.45-1.65	7.1	8.3	8.1	8.1	0.3 - 0.5	7.1	8.5	7.5	7.5
1.65-1.85	7.2	7.7	8.0	8.0	0.5 - 0.75	7.2	7.1	7.3	7.3

1.85-2.1	7.1	7.3	7.5	7.5	0.75 - 1.05	7.1	7.3	7.3	7.3
Normalization	4.9	3.8	3.0	3.0	Normalization	4.9	3.8	3.0	3.0

Table 11. Total systematic uncertainty of the *Λ* yield for 4.5 AGeV.

Target / **Interval**	***y***				**Target** / **Interval**	***p_T***			
	C, sys%	***Al***, sys%	***Cu***, sys%	***Pb***, sys%		***C***, sys%	***Al***, sys%	***Cu***, sys%	***Pb***, sys%
1.2-1.45	12.8	12.8	12.9	12.9	0.1-0.3	12.8	13.4	13.4	13.6
1.45-1.65	13.0	13.1	13.4	13.3	0.3-0.5	12.9	13.9	14.4	14.4
1.65-1.85	14.7	13.0	13.3	12.8	0.5-0.75	12.8	13.2	13.1	14.0
1.85-2.1	13.0	12.9	13.3	12.9	0.75-1.05	12.9	12.8	12.9	13.0
Normalization	4.9	3.8	3.0	3.0	Normalization	4.9	3.8	3.0	3.0

Integrated yields and cross sections

The integrated yields of *Λ* hyperons produced in the kinematic range of $0.1<p_T<1.05$ GeV/*c* and $1.2 <y<2.1$ in minimum bias *C+C, Al, Cu, Pb* interactions, the extrapolation of the measured yields to the full kinematic range the predictions of the DCM-QGSM and URQMD, the model extrapolation factors, reconstruction efficiencies, the inverse slopes extracted from fits to the invariant p_T spectra, the estimated yields and inclusive cross sections of the *Λ* hyperon production in *C+C, C+Al, C+Cu, C+Pb* minimum bias interactions with beam energies of 4.0 and 4.5 AGeV are summarized in Tables 12 and 13.

Table 12. Extrapolation factors to the full kinematic range, reconstruction efficiencies, *Λ* hyperon yields and cross sections for 4.0 AGeV data. The first error given is statistical, the second error is systematic.

4.0 AGeV	***C***	***Al***	***Cu***	***Pb***
DCM-QGSM & URQMD extrap. factor (average)	2.48	3.02	4.02	6.83
Efficiency in $0.1<p_T<1.05$ GeV/c, $1.2<y_{lab}<2.1$	0.032	0.027	0.024	0.019
Yields in $0.1<p_T<1.05$ GeV/c, $1.2<y_{lab}<2.1$	0.011±0.003±0.001	0.026±0.007±0.002	0.030±0.006±0.003	0.039±0.015±0.002
Yields in the full kin. range *Npart / Ncoll* DCM-QGSM	0.027±0.007±0.003 9 / 5	0.079±0.021±0.006 13.4 / 9.3	0.121±0.025±0.012 23 / 18	0.266±0.102±0.014 50.5 / 52.5
Λ cross section in min. bias interact, mb	22.4 ± 5.8 ± 4.2	99.5 ± 26.5 ± 7.6	216.6 ± 44.8 ± 21.5	818.0 ± 303.7 ± 43.1
Inverse slope parameter, MeV	114 ± 19 ± 4	108 ± 16 ± 4	96 ± 14 ± 1	83± 8 ± 1

Table 13. Extrapolation factors to the full kinematic range, reconstruction efficiencies, *Λ* hyperon yields and cross sections for 4.5 AGeV data. The first error given is statistical, the second error is systematic.

4.5 AGeV	***C***	***Al***	***Cu***	***Pb***
DCM-QGSM & URQMD extrap. factor (average)	2.32	2.85	3.67	5.99
Efficiency in $0.1<p_T<1.05$ GeV/c, $1.2<y_{lab}<2.1$	0.028	0.024	0.019	0.015

Yields in $0.1 < p_T < 1.05$ GeV/c, $1.2 < y < 2.1$	0.013±0.004±0.001	0.023±0.006±0.003	0.037±0.007±0.006	-
Yields in the full kin. range *Npart / Ncoll* DCM-QGSM	0.030±0.009±0.002 9 / 5	0.066±0.017±0.009 13.4 / 9.3	0.136±0.026±0.022 23 / 18	-
Λ cross section in min. bias interact., mb	25.0 ± 7.5 ± 4.2	83.2 ± 21.4 ± 25.2	243.4 ± 46.5 ± 39.4	-
Inverse slope parameter, MeV	116 ± 24 ± 1	115 ± 7 ± 5	101 ± 3 ± 0,1	-

In general, the transport models describe the shape of the differential spectra on y^* and p_T, but predict more abundant yields of *Λ* hyperons than measured in the experiment. The UrQMD model predictions are closer to the experimental data in the normalization than the predictions of the DCM-QGSM and PHSD models. The PHSD model predicts a stronger rise of the *Λ* hyperon yields in the BM@N kinematic range with the atomic weight of the target than the DCM-QGSM and UrQMD models. This tendency is deduced from the rapidity spectra of *Λ* hyperons generated in the models which are shown in Fig.36.

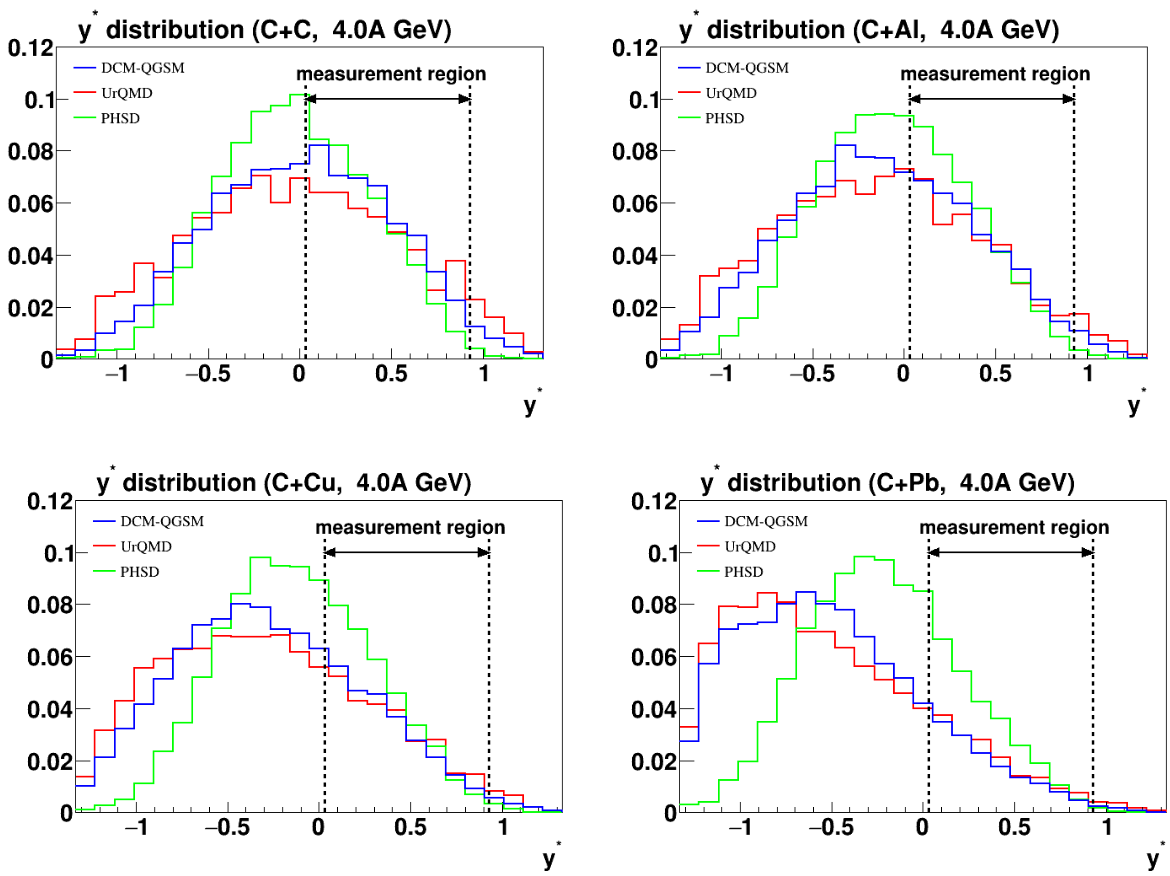

Figure 36. Rapidity spectra of *Λ* hyperons in minimum bias interactions of 4.0 AGeV carbon beam with *C, Al, Cu, Pb* targets, generated with the DCM-QGSM, UrQMD and PHSD models. The BM@N measurement range in y* is indicated.

The *Λ* yields and production cross sections in *C+C* interactions can be compared with the previous results of the 23.2±2.5 mb [10] and 24±6 mb [11] measured in interactions of the carbon beam with the momentum of 4.2 GeV/*c* per nucleon (beam kinetic energy of 3.36 AGeV per nucleon) with the Propane Chamber experiment, as well as with the result of the HADES experiment at 2.0 AGeV. In Table 14 yields and inclusive cross sections of *Λ* hyperon production in interactions of light and medium nucleus from the other experiments are presented for the comparison.

Table 14. Yields and inclusive cross sections of *Λ* hyperon production in interactions of light and medium nucleus.

Interacting nucleus / reference	**Beam momentum, kinetic energy (E_{kin})**	***Λ* cross section, mb**	***Λ* yield, $\cdot 10^{-2}$**
He_4+Li_6	4.5 GeV/c (3.66 AGeV)	5.9± 1.5	1.85 ± 0.5
C+C	4.2 GeV/c (3.36 AGeV)	24 ± 4	2.89±0.72
C+C, propane Chamber	4.2 GeV/c (3.36 AGeV)	23.2±2.5	2.8 ± 0.3
p+p	4.95 GeV/c (4.1 AGeV)		2.3 ± 0.4
C+C, HADES	2.0 AGeV	$8.7\pm1.1\pm^{3.2}_{1.67}$	$0.92\pm0.12\pm^{0.34}_{0.17}$
Ar+KCl, HADES	1.76 AGeV		3.93±0.14±0.15
Ar+KCl, FOPI	1.93 AGeV		3.9±0.14±0.08
Ni+Ni, FOPI, central 390 mb from 3.1 *b*	1.93 AGeV		$0.137\pm0.005\pm^{0.009}_{0.025}$
Ni+Cu, EOS, full *b*<8.9 fm / central *b*<2.4 fm	2.0 AGeV	112±24 / 20±3	
Ar+KCl, central *b*<2.4 fm	1.8 AGeV	7.6±2.2	

Table 15. *Λ* hyperon yields and yields normalized to the number of nucleons-participants. The first error is statistical, the second error is systematic. Predictions of the DCM-QGSM, UrQMD and PHSD models are shown for *C+C* interactions at different beam energies.

C+C	**4.5 AGeV**	**4.0 AGeV**	**3.5 AGeV**	**2.0 AGeV**
BM@N yield Npart / Ncoll Yield normal to N_{part} Yield normal to N_{coll}	0.030±0.009±0.002 9 / 5 = 1.8 (3.33±1.0±0.22)×10^{-3} (6.0±1.8±0.4) ×10^{-3}	0.027±0.007±0.003 9 / 5 = 1.8 (3.0±0.78±0.33) ×10^{-3} (5.4±1.4±0.6) ×10^{-3}		
DCM-QGSM DCM-QGSM / N_{part} DCM-QGSM / N_{col}	0.157 17.44×10^{-3} 31.14×10^{-3}	0.117 13.0·10^{-3} 23.4·10^{-3}	0.0771 8.57×10^{-3} 15.43×10^{-3}	0.0125 1.39×10^{-3} 2.50×10^{-3}
UrQMD yield UrQMD / N_{part} UrQMD / N_{coll}	0.09 10.0×10^{-3} 18.0×10^{-3}	0.069 7.67×10^{-3} 13.8×10^{-3}	0.0577 6.41×10^{-3} 11.54×10^{-3}	0.0118 1.31×10^{-3} 2.36×10^{-3}
PHSD yield PHSD / N_{part} PHSD / N_{coll}	0.127 14.11×10^{-3} 25.4×10^{-3}	0.092 10.22×10^{-3} 18.4×10^{-3}	0.0684 7.6×10^{-3} 13.7×10^{-3}	0.0119 1.32×10^{-3} 2.38×10^{-3}
Other Experiments			0.0289±0.0072 (3.36AGeV) 0.028±0.003 (3.36 AGeV) Propane Chamber	$0.0092\pm0.0012\pm^{0.0034}_{0.0017}$ HADES

Table 16. *Λ* hyperon yields and yields normalized to the number of nucleons-participants. The first error is statistical, the second error is systematic. Predictions of the DCM-QGSM, UrQMD and PHSD models are shown for carbon-nucleus interactions at different beam energies.

C+Al	**4.5 AGeV**	**4.0 AGeV**	**3.5 AGeV**
BM@N yield	0.066±0.017±0.009	0.079±0.021±0.006	
Npart / Ncoll	13.4 / 9.3 = 1.441	13.4 / 9.3 = 1.441	
Yield normal to N_{part}	(4.93±1.27±0.67) ×10^{-3}	(5.9±1.57±0.45) ×10^{-3}	
Yield normal to N_{coll}	(7.1±1.83±0.97) ×10^{-3}	(8.49±2.26±0.65) ×10^{-3}	
DCM-QGSM	0.235	0.169	0.115
QGSM / N_{part}	17.54×10^{-3}	12.61×10^{-3}	8.58×10^{-3}
QGSM / N_{coll}	25.27×10^{-3}	18.17×10^{-3}	12.41×10^{-3}
UrQMD yield	0.135	0.111	0.092
UrQMD / N_{part}	10.07×10^{-3}	8.28×10^{-3}	6.87×10^{-3}
UrQMD / N_{coll}	14.52×10^{-3}	11.94×10^{-3}	9.89×10^{-3}
PHSD yield	0.168	0.134	0.098
PHSD / N_{part}	12.54×10^{-3}	10.0×10^{-3}	7.31×10^{-3}
PHSD / N_{coll}	18.06×10^{-3}	14.41×10^{-3}	10.54×10^{-3}
C+Cu	**4.5 AGeV**	**4.0 AGeV**	**3.5 AGeV**
BM@N yield	0.136±0.026±0.022	0.121±0.025±0.012	
Npart / Ncoll	23 / 18 = 1.278	23 / 18 = 1.278	
Yield normal to N_{part}	(5.91±1.33±0.96) ×10^{-3}	(5.26±1.09±0.52) ×10^{-3}	
Yield normal to N_{coll}	(7.56±1.44±1.22) ×10^{-3}	(6.72±1.39±0.67) ×10^{-3}	
DCM-QGSM	0.346	0.251	0.178
QGSM / N_{part}	15.04×10^{-3}	10.91×10^{-3}	7.74×10^{-3}
QGSM / N_{coll}	19.22×10^{-3}	13.94×10^{-3}	9.89×10^{-3}
UrQMD yield	0.2	0.172	0.137
UrQMD / N_{part}	8.7×10^{-3}	7.48×10^{-3}	5.96×10^{-3}
UrQMD / N_{coll}	11.11×10^{-3}	9.56×10^{-3}	7.61×10^{-3}
PHSD yield	0.243	0.192	0.145
PHSD / N_{part}	10.57×10^{-3}	8.35×10^{-3}	6.3×10^{-3}
PHSD / N_{coll}	13.5×10^{-3}	10.67×10^{-3}	8.06×10^{-3}
C+Pb	**4.5 AGeV**	**4.0 AGeV**	**3.5 AGeV**
BM@N yield	-	0.266±0.102±0.014	
Npart / Ncoll	52.5 / 50.5 = 0.962	52.5 / 50.5 = 0.962	
Yield normal to N_{part}	-	(5.07±1.94±0.27) ×10^{-3}	
Yield normal to N_{coll}	-	(5.27±2.02±0.28) ×10^{-3}	
DCM-QGSM	0.507	0.365	0.277
QGSM / N_{part}	9.66 ×10^{-3}	6.95·10^{-3}	5.28×10^{-3}
QGSM / N_{coll}	10.04 ×10^{-3}	7.23·10^{-3}	5.49×10^{-3}
UrQMD yield	0.341	0.314	0.222
UrQMD / N_{part}	6.49×10^{-3}	5.98×10^{-3}	4.23×10^{-3}
UrQMD / N_{coll}	6.75×10^{-3}	6.22×10^{-3}	4.4×10^{-3}
PHSD yield	0.38	0.303	0.226
PHSD / N_{part}	7.24×10^{-3}	5.77×10^{-3}	4.3×10^{-3}
PHSD / N_{coll}	7.52×10^{-3}	6.0×10^{-3}	4.48×10^{-3}

The BM@N result for the Λ yield in *C+C* minimum bias interactions is compared with the results taken from other experiments [9], [10], [11]. The *C+C* data was also compared with predictions of the DCM-QGSM, UrQMD and PHSD transport models (Fig. 37 and Table 15) for the C+C interactions. There is a general tendency that the transport models predict a faster rise of the Λ hyperon yield with the energy in comparison with the experimental data.

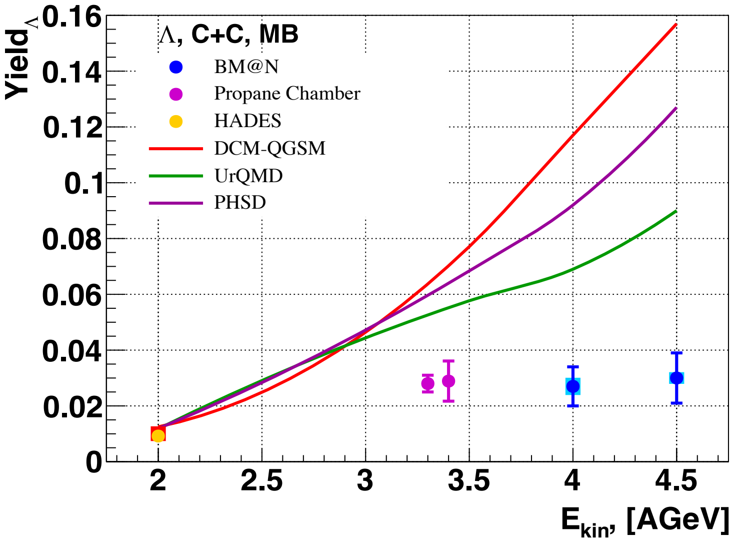

Figure 35. Energy dependence of *Λ* yields measured in different experiments. The error bars represent the statistical errors, the blue bands show the systematic errors. BM@N result is compared with data taken from another experiments [9], [10], [11]. The predictions of the DCM-QGSM, UrQMD and PHSD models are shown as colored lines.

The energy dependences of the *Λ* yields measured in BM@N are presented in Table 16 and Figure 38 for *C+Al, C+Cu, C+Pb* minimum bias interactions, respectively. The predictions of the transport models are shown. In general, the model predictions exceed the experimental data in the normalization. The DCM-QGSM model predicts a higher full yield of *Λ* hyperons than the two other models.

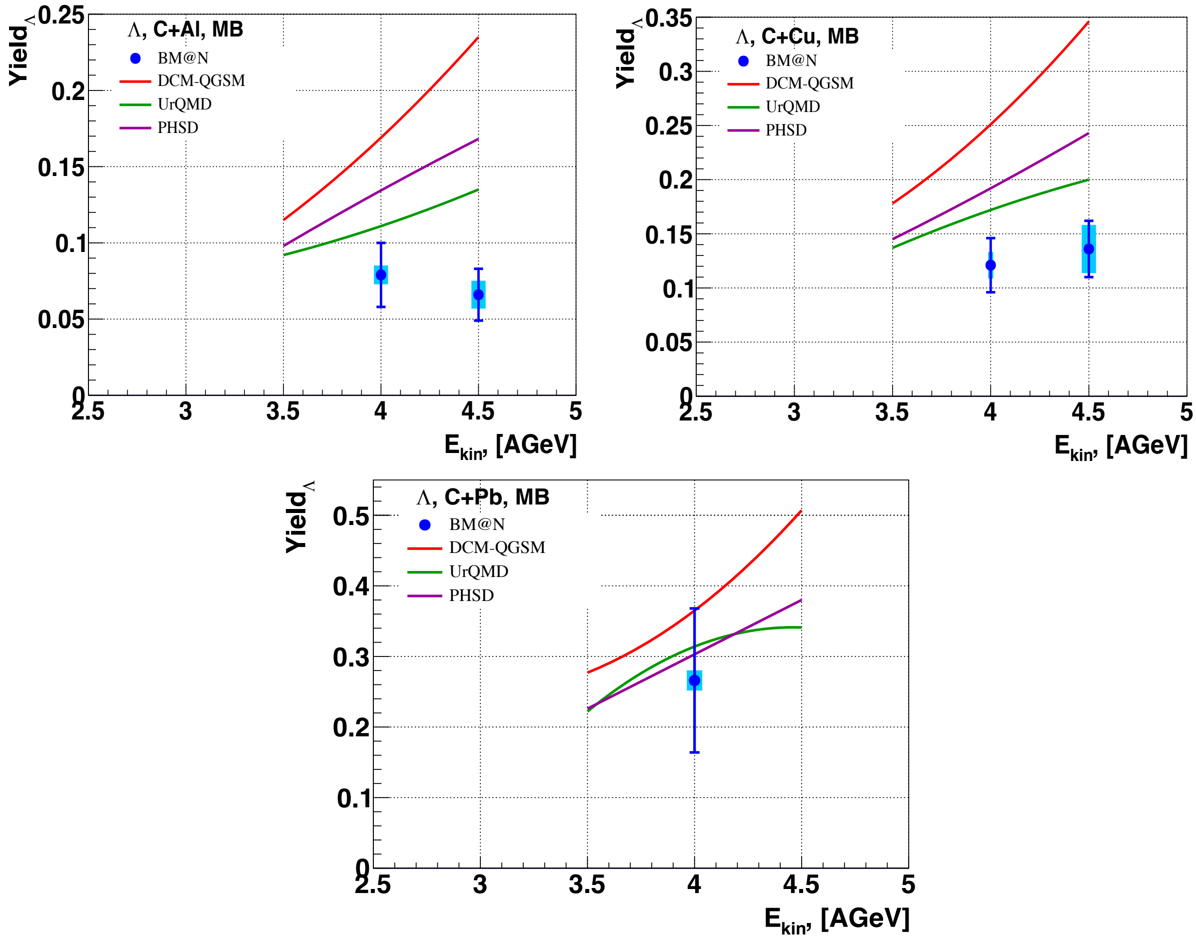

Figure 38. Energy dependence of *Λ* yields measured in BM@N experiment for the minimum bias interactions. The error bars represent the statistical errors, the blue bands show the systematic errors. The predictions of the DCM-QGSM, UrQMD and PHSD models are shown as colored lines.

To compare yields of particle production in nucleus-nucleus interactions, they are usually normalized to the mean number of nucleons participating in interactions (participants). The numbers of participants in minimum bias *C+C, C+Al, C+Cu, C+Pb* interactions are estimated using the DCM-QGSM model [12]. The results (*A1+A2*) are shown in Table 17.

Table 17. Number of participants in minimum bias *A+A* events at 4.0A GeV

A_1A_2	A_1	A_2	$A_1 + A_2$
C+C	4.5	4.5	9.0
C+Al	5.23	8.14	13.37
C+Cu	6.21	16.79	23.0
C+Pb	7.33	43.15	50.48

The ratios of the Λ hyperon yields to the number of nucleons-participants measured in BM@N carbon-nucleus interactions are presented in Fig. 39 and Tables 15-16.

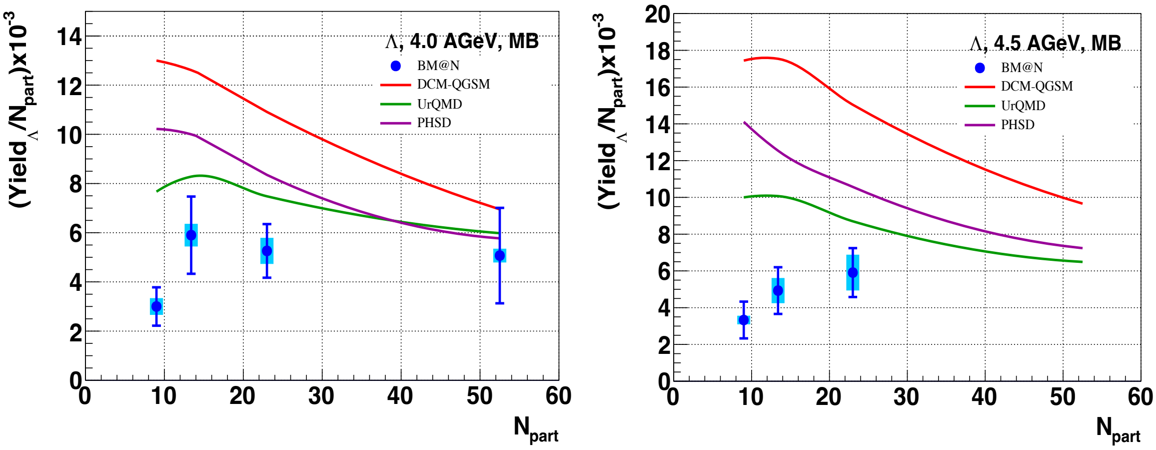

Figure 39. Ratios of the Λ hyperon yields to the number of nucleons-participants measured in BM@N carbon-nucleus interactions at 4.0 AGeV (left) and 4.5 AGeV (right). The error bars represent the statistical errors, the blue bands show the systematic errors. The predictions of the DCM-QGSM, UrQMD and PHSD models are shown as colored lines.

Summary

Production of Λ hyperons in interactions of the carbon beam with *C, Al, Cu, Pb* targets was studied with the BM@N detector. The analysis procedure is described including details of the Λ hyperon reconstruction, efficiency and systematic uncertainty evaluation. The physics results are presented for Λ hyperon yields and cross sections in minimum bias carbon-nucleus interactions at the beam kinetic energies of 4.0 and 4.5 AGeV. They are compared with models of nucleus-nucleus interactions and with the results of other experiments studied carbon-nucleus interactions at lower energies.

Bibliography

[1] http://bmnshift.jinr.ru/wiki/lib/exe/fetch.php?media=tdr_gem_may2017_v1.doc
[2]http://bmnshift.jinr.ru/wiki/lib/exe/detail.php?id=run_5_december_2016&media=setting_1_f.jpg
[3] D.Baranov et al., First Results from BM@N Technical Run with Deuteron Beam, Phys. Part. Nucl. Lett. 15, no. 2, 148 (2018)
[4] V. Akishina and I. Kisel. Time-based cellular automaton track finder for the CBM experiment - 2015. J. Phys.: Conf. Ser. 599, 012024
[5] S. Gorbunov and I. Kisel. Reconstruction of decayed particles based on the Kalman filter - 2007. CBM-SOFTnote—003

[6] K. Alishina, Yu. Yu. Stepanenko, A. Y. Khukhaeva. GEM residuals correction in Monte-Carlo simulation for the Run-6 of the BM@N experiment Physics of Particles and Nuclei Letters, 2022, Vol. 19, No. 5, pp. 485–488. © Pleiades Publishing, Ltd., 2022. ISSN 1547-477.
[7] Study of Λ-hyperon production in collisions of the heavy ions with solid targets in the BM@N experiment. K. Alishina, Yu. Yu. Stepanenko. Physics of Particles and Nuclei Letters, 2024, Vol. 21, No. 4, pp. 683–686. © Pleiades Publishing, Ltd., 2024. ISSN 1547-4771.
[8] H.Angelov et al., P1-80-473, JINR, Dubna
[9] Kalliopi Kanaki, PhD "Study of Λ hyperon production in *C+C* collisions at 2A GeV beam energy with the HADES spectrometer", 2007
[10] D.Armutlijsky et al., Report No, P1-85-220, JINR, Dubna
[11] S.Arakelian et al., Report No, P1-83-354, JINR, Dubna
[12] Result of Genis Musulmanbekov, private communication